

Extracting Koopman Operators for Prediction and Control of Non-linear Dynamics Using Two-stage Learning and Oblique Projections

Daisuke Uchida¹ and Karthik Duraisamy¹

¹Department of Aerospace Engineering, University of Michigan

Abstract

The Koopman operator framework provides a perspective that non-linear dynamics can be described through the lens of linear operators acting on function spaces. As the framework naturally yields linear embedding models, there have been extensive efforts to utilize it for control, where linear controller designs can be applied to control possibly nonlinear dynamics. However, it is challenging to successfully deploy this modeling procedure in a wide range of applications. In this work, some of the fundamental limitations of linear embedding models are addressed. We show a necessary condition for a linear embedding model to achieve zero modeling error, highlighting a trade-off relation between the model expressivity and a restriction on the model structure to allow the use of linear systems theories for nonlinear dynamics. To achieve good performance despite this trade-off, neural network-based modeling is proposed based on linear embedding with oblique projection, which is derived from a weak formulation of projection-based linear operator learning. We train the proposed model using a two-stage learning procedure, wherein the features and operators are initialized with orthogonal projection, followed by the main training process in which test functions characterizing the oblique projection are learned from data. The first stage achieves an optimality ensured by the orthogonal projection and the second stage improves the generalizability to various tasks by optimizing the model with the oblique projection. We demonstrate the effectiveness of the proposed method over other data-driven modeling methods by providing comprehensive numerical evaluations where four tasks are considered targeting three different systems.

1 Introduction

Data-driven approaches[7] to the modeling and control of dynamical systems have been gaining attention and popularity in recent years. Among many different data-driven modeling frameworks, the Koopman operator is emerging as a promising tool that can represent a nonlinear dynamical system as a linear one in a higher (possibly infinite) dimensional embedded space. In addition to theoretical works concerning the development of computational methods to estimate the Koopman operator[8, 34, 41, 6], a number of applications in various fields have been also reported in the literature in recent years[33, 15, 16, 4]. While the numerical estimation of the spectral properties of the Koopman operator has been one of the central topics (e.g., [35, 28, 12, 11]), there have been also many efforts that extend the Koopman operator framework to systems with control inputs[44, 56, 5].

After a formal extension of the Koopman operator formalism to general non-autonomous systems was established in [26], various types of controller design problems have been addressed. The most

notable feature of this framework is that linear control theories are utilized to control possibly nonlinear dynamics, whose governing equations are even unknown. Linear Quadratic Regulator (LQR) is one of the simplest designs that may be adopted in this scenario and several studies showed its applicability and effectiveness in both simulations and real experiments targeting robotic systems[31, 32, 18]. Linear Model Predictive Control (MPC) is currently the most popular choice of Koopman-based controller design and a number of papers address linear MPC design problems to control nonlinear dynamics based on this framework[26, 36, 1, 47, 49, 48, 59]. Several other works combine the data-driven Koopman operator framework with different tools, e.g., eigenfunctions of the Koopman operator[22], control barrier functions[13], and switching time optimization[43].

While many Koopman-based controller designs have been developed thus far, challenges and difficulties persist, especially in accurately representing the non-autonomous dynamics using the Koopman operator. Extended Dynamic Mode Decomposition (EDMD)[55], which is a linear regression type of method to compute a finite-dimensional approximation of the Koopman operator, is widely used in the modeling phase. However, it is known that its convergence property to the true Koopman operator does not hold for non-autonomous systems[26]. This implies that collecting a sufficiently large number of observables and data points may not necessarily lead to better model accuracy. Thus, one may not be able to establish a reliable theoretical basis for the use of the Koopman operator for modeling the unknown, non-autonomous dynamics. In addition to this convergence issue, the nature of data-driven problem settings also renders the occurrence of the modeling error unavoidable. For instance, model training can yield biased or poor results if the data is obtained only from very limited operating points or the amount of data is too small.

To tackle the incompleteness of EDMD-based modeling, robust controller designs have been integrated into the Koopman framework. In [59], a robust Koopman MPC design is proposed on the basis of EDMD and tube-based MPC that accounts for both modeling error and additive disturbances. An off-set free MPC framework was combined with Koopman Lyapunov-based MPC, which also takes the modeling error of EDMD approximation into account[49]. Another robust controller design utilizes an \mathcal{H}_2 norm characterization of discrete-time linear systems to represent the modeling error of EDMD models using polytope sets[54]. Despite these efforts focused on the controller design aspect, the fact that EDMD often fails to accurately reproduce the behavior of complex nonlinear dynamics may become an issue. Indeed, state prediction is one of the most basic yet essential tasks from a modeling perspective.

When EDMD-based methods do not result in satisfactory model accuracy, one may resort to using more expressive schemes such as neural networks to learn observables or feature maps from data. The use of neural networks in Koopman-based modeling has been shown to be promising in many studies (e.g., [42, 51, 30, 58, 40]). Specifically, neural network-based models can be considerably more expressive than EDMD models and it is expected that they can address more challenging dynamical systems such as those with high degrees of nonlinearities and large dimensions. This strategy can be also adopted in control applications and various papers developed data-driven Koopman-based controller designs with neural networks[19, 20, 57, 53].

Although the use of neural networks may be a more preferable choice that yields expressive and flexible models, issues concerning the modeling error can hinder the successful application of Koopman-based modeling. Compared to EDMD, learning with neural networks is generally more sensitive to the quality of data as well as other factors in the learning procedure since it is a high-dimensional non-convex optimization with many learnable parameters. As a result, neural network-based models may be prone to overfitting or poor learning due to biased data-collecting procedures or lack of data. In [19], a probabilistic neural network is adopted to introduce the uncertainty of modeling as an additive noise to the dynamics and a nominal controller is compensated by an additional control input. Reference [53] points out that the modeling error regarding closed-loop

dynamics may be more difficult to manage than that of state prediction. Based on this fact, a model refinement technique was proposed that incorporates data points collected from a closed-loop dynamics into neural network training to directly mitigate the modeling error in the closed-loop environment.

Given the large number of Koopman operator learning approaches in the literature, it remains a challenge to ensure that the learned model is not just capable of predicting the behavior of a nonlinear dynamics accurately, but is also amenable to many types of tasks such as controller design and decision-making. The present work is focused on the use of oblique projection in a Hilbert space to develop a new linear operator-based data-driven modeling method. The concept of projection has been used and proven to be useful in other disciplines of dynamical systems modeling[2, 10]. It also appears in the formulations of the data-driven Koopman operator-based modeling. EDMD can be considered as an algorithm to compute the orthogonal projection of the action of the Koopman operator in the L_2 space endowed with the empirical measure supported on the given data points[23, 27]. This is also termed the Galerkin projection or Galerkin approximation of the Koopman operator in the literature[41, 24]. While this perspective is mostly adopted in theoretical analyses of EDMD or when the EDMD procedure is introduced, there are few works that utilize the concept of projection directly to develop Koopman operator-based data-driven methods.

This paper develops a new data-driven modeling method by reformulating a problem of dynamical systems modeling as projection-based linear operator-learning in a Hilbert space. A notable feature of the proposed method is that its model structure is considered an extension of EDMD. Consider a discrete-time, non-autonomous system $\chi^+ = F(\chi, u)$, where $\chi \in \mathcal{X} \subseteq \mathbb{R}^n$, $u \in \mathcal{U} \subseteq \mathbb{R}^p$, $\chi^+ \in \mathcal{X}$, and $F : \mathcal{X} \rightarrow \mathcal{X}$ are the state, the input, their corresponding successor, and a nonlinear mapping describing the dynamics, respectively. Given feature maps or observables $g_i : \mathcal{X} \rightarrow \mathbb{R}$ ($i = 1, \dots, N_x$) and a data set $\{(\chi_i, u_i, y_i) \mid y_i = F(\chi_i, u_i), \chi_i \in \mathcal{X}, u_i \in \mathcal{U}, i = 1, \dots, M\}$, we consider the following dynamic model that fits the data:

$$\begin{bmatrix} g_1(y_i) \\ \vdots \\ g_{N_x}(y_i) \end{bmatrix} \approx \mathbf{A} \begin{bmatrix} g_1(\chi_i) \\ \vdots \\ g_{N_x}(\chi_i) \end{bmatrix} + \mathbf{B}u_i, \quad i = 1, \dots, M,$$

which is formally introduced as a linear embedding model in Section 2.1 (Eq. (2)). Note that the dynamics of this model is represented in the embedded state $[g_1(\chi), \dots, g_{N_x}(\chi)]^T \in \mathbb{R}^{N_x}$, rather than the original state $\chi \in \mathbb{R}^n$. The standard EDMD solves a linear regression problem that minimizes the sum of squared errors over the given data points. This yields the model parameters $[\mathbf{A} \ \mathbf{B}]$ as its unique least square solution, which depends on the design of the feature maps g_i . In the proposed method, we extend this structure of $[\mathbf{A} \ \mathbf{B}]$ in a way that they are not only dependent on the feature maps g_i , but also test functions $\varphi_i : \mathcal{X} \times \mathcal{U} \rightarrow \mathbb{R}$, ($i = 1, \dots, \hat{N}$), which are introduced by the idea of oblique projection in the context of linear operator-learning in a Hilbert space.

A major difference between the proposed method and EDMD, in addition to the different structures of $[\mathbf{A} \ \mathbf{B}]$, is that the feature maps g_i and the test functions φ_i are learned from data in the proposed method, whereas EDMD seeks $[\mathbf{A} \ \mathbf{B}]$, with user-specified feature maps g_i . Since the new structure of $[\mathbf{A} \ \mathbf{B}]$ includes the test functions φ_i as additional tunable parameters, it allows for flexibility of the model, which could, in turn, lead to better accuracy and generalizability of the model. Optimizing oblique projections has been also found to yield better performance in the context of reduced-order modeling[39, 21]. Whereas [39, 21] seek to find optimal subspaces that define the oblique projection, we directly parameterize the feature maps and the test functions and implement the model learning as neural network training. As shown in Fig. 1, the generalizability of our modeling method is evaluated by two factors in this paper: different dynamical systems; and

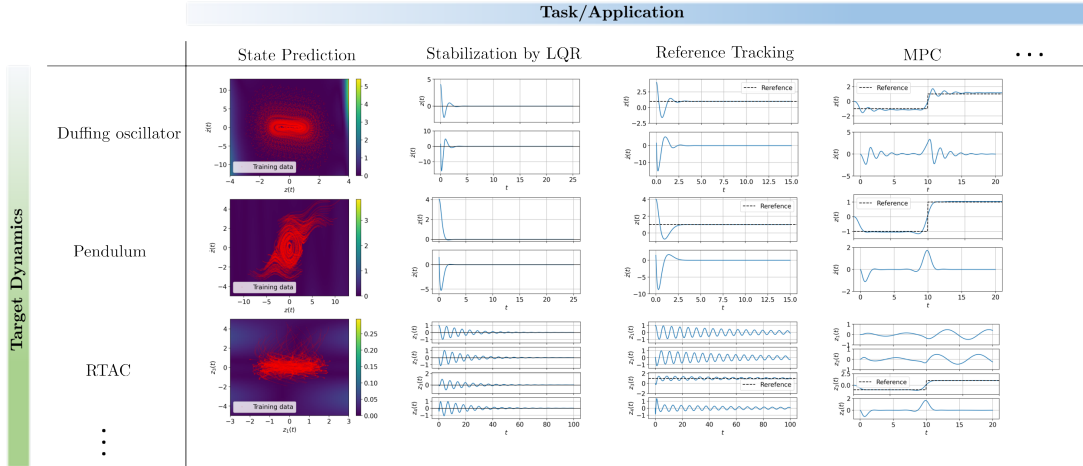


Fig. 1: Chart showing the matrix of examples and tasks to assess generalizability of the present approach.

the range of tasks the model can be applied to. We provide comprehensive numerical evaluations that compare the generalizability of different data-driven models using four tasks: state prediction, stabilization by LQR, reference tracking, and linear MPC, each of which targets three nonlinear dynamical systems: the Duffing oscillator, the simple pendulum, and the Rotational/Translational Actuator (RTAC).

In Section 2, we formally introduce a problem of data-driven modeling for discrete-time, non-autonomous systems and show that while the linear embedding model leads to an advantage that linear controller designs in the embedded space can be applied to control possibly nonlinear dynamics, it may suffer from fundamental limitations to realize accurate data-driven models. In Section 3, the same problem is reformulated in the context of projection-based linear operator learning in a Hilbert space and the EDMD operator is generalized to the one that is derived based on a weak formulation obtained by oblique projection. In Section 4, learning problems are formulated to train the proposed model, where neural networks are used to characterize both the feature maps and the test functions. Numerical analyses are provided in Section 5 to show the capability and generalizability of the proposed method. In addition to the predictive accuracy of the model, three different control applications: stabilization by LQR, reference tracking, and linear MPC are considered and the proposed modeling method is compared to other Koopman-based data-driven models.

2 Linear Embedding Models for Nonlinear Dynamics

2.1 Defining the Modeling Problem

This section introduces a problem of data-driven modeling for a discrete-time dynamical system:

$$\chi^+ = F(\chi, u), \quad \chi \in \mathcal{X} \subseteq \mathbb{R}^n, \quad u \in \mathcal{U} \subseteq \mathbb{R}^p, \quad F: \mathcal{X} \times \mathcal{U} \rightarrow \mathcal{X}, \quad (1)$$

where χ is an n dimensional state in the state space \mathcal{X} , u is an input from the admissible set \mathcal{U} of inputs to the system, χ^+ is the successor corresponding to χ and u , and F is a possibly nonlinear

map describing the dynamics, respectively. It is assumed throughout the paper that the explicit knowledge of F is not available and a model that reproduces the dynamics (1) is obtained only from data of the form $\{(\chi^+, \chi, u) \mid \chi^+, \chi, \text{ and } u \text{ satisfy (1)}\}$.

We introduce N_x feature maps $g_i : \mathcal{X} \rightarrow \mathbb{R}$ ($i = 1, \dots, N_x$), which are functions from the state space \mathcal{X} to \mathbb{R} , and consider approximating the unknown dynamics (1) by a linear operator $[\mathbf{A} \ \mathbf{B}]$ s.t.

$$\begin{cases} \begin{bmatrix} g_1(\chi^+) \\ \vdots \\ g_{N_x}(\chi^+) \end{bmatrix} \approx [\mathbf{A} \ \mathbf{B}] \begin{bmatrix} g_1(\chi) \\ \vdots \\ g_{N_x}(\chi) \\ u \end{bmatrix} = \mathbf{A} \begin{bmatrix} g_1(\chi) \\ \vdots \\ g_{N_x}(\chi) \end{bmatrix} + \mathbf{B}u, \\ \chi^+ \approx \omega \left(\begin{bmatrix} g_1(\chi^+) \\ \vdots \\ g_{N_x}(\chi^+) \end{bmatrix} \right), \end{cases} \quad (2)$$

where $\mathbf{A} \in \mathbb{R}^{N_x \times N_x}$ and $\mathbf{B} \in \mathbb{R}^{N_x \times p}$ are matrices and $\omega : \mathbb{R}^{N_x} \rightarrow \mathbb{R}^n$ denotes a decoder from the embedded state $[g_1(\chi) \cdots g_{N_x}(\chi)]^\top$, which is characterized by the feature maps g_i , to the original state χ . We call (2) a linear embedding model in this paper. It is a common control model architecture in the Koopman literature, which has several unique features:

1. The model is represented in an N_x dimensional embedded space, which is characterized by the nonlinear feature maps g_i .
2. The model dynamics in the embedded space is linear and is governed by the linear operator $[\mathbf{A} \ \mathbf{B}]$.
3. While nonlinearity w.r.t. the state χ can be introduced through the feature maps g_i , the model is strictly linear w.r.t. the input u (Being strictly linear w.r.t. u implies that the term involving u is given in the form $\mathbf{B}u$, where \mathbf{B} is a constant matrix).

The linear dynamics structure in the embedded space is especially advantageous when one uses the data-driven modeling method for control. For simplicity, if the first n feature maps are defined as the state $\chi \in \mathbb{R}^n$ itself so that $[g_1(\chi) \cdots g_n(\chi)]^\top := \chi$, the above equations can be written as

$$\begin{bmatrix} \chi^+ \\ g_{n+1}(\chi^+) \\ \vdots \\ g_{N_x}(\chi^+) \end{bmatrix} \approx \mathbf{A} \begin{bmatrix} \chi \\ g_{n+1}(\chi) \\ \vdots \\ g_{N_x}(\chi) \end{bmatrix} + \mathbf{B}u, \quad (3)$$

where the decoder ω need not be explicitly defined since the first n components of the embedded state correspond to the prediction of the state χ^+ . The above equation implies that linear controller designs can be utilized to control possibly nonlinear dynamics (1) by viewing (3) as a Linear Time-Invariant (LTI) system in a new coordinate $[\chi^\top \ g_{n+1}(\chi) \cdots g_{N_x}(\chi)]^\top$. For instance, stabilization of the original dynamics (1) may be achieved by designing an LQR that stabilizes the LTI system (3) since $[\chi^\top \ g_{n+1}(\chi) \cdots g_{N_x}(\chi)]^\top \rightarrow 0$ implies $\chi \rightarrow 0$.

On the other hand, the validity of this model w.r.t. the target dynamics (1) may need to be established in practice since its construction is based on specific model structures as stated

above, which in general limit the performance of the model for a wide range of dynamical systems. Specifically, the modeling error, which is not yet stated in (2) or (3) explicitly since the approximate equal sign \approx is used instead, may become so dominant that the model will be no longer valid or reasonable to approximate the unknown dynamics (1).

2.2 Koopman Operator

The Koopman operator[25], which is a type of linear operator acting on a function space, is well-known as a promising mathematical tool that may be able to justify the use of linear embedding models introduced in the previous section as well as serve as a basis to develop methods to learn such models from data. For an autonomous system s.t.

$$\chi^+ = f(\chi), \quad f: \mathcal{X} \rightarrow \mathcal{X}, \quad (4)$$

the Koopman operator $\mathcal{K}: \mathcal{F} \rightarrow \mathcal{F}$ is defined as a linear operator s.t.

$$\mathcal{K}g = g \circ f \Leftrightarrow (\mathcal{K}g)(\chi) = g(f(\chi)), \quad g \in \mathcal{F}, \quad \chi \in \mathcal{X}, \quad (5)$$

where \mathcal{F} is a space of functions and its elements $g: \mathcal{X} \rightarrow \mathbb{R}$ may be considered as feature maps introduced in the previous section. In the Koopman literature, g are also referred to as observables. From (5), it is easily seen that the Koopman operator \mathcal{K} plays a role in describing the r.h.s. of autonomous dynamics (4) in the function space \mathcal{F} instead of the state space \mathcal{X} as

$$g(\chi^+) = g(f(\chi)) = (\mathcal{K}g)(\chi). \quad (6)$$

Moreover, if we consider the same type of model representation as (2) but ignoring the input effect:

$$\begin{bmatrix} g_1(\chi^+) \\ \vdots \\ g_{N_x}(\chi^+) \end{bmatrix} \approx \mathbf{A} \begin{bmatrix} g_1(\chi) \\ \vdots \\ g_{N_x}(\chi) \end{bmatrix}, \quad (7)$$

this model can be naturally derived from a finite-dimensional approximation of the Koopman operator \mathcal{K} by the following proposition.

Proposition 1. Suppose $g_i \in \mathcal{F}$ ($i = 1, \dots, D$, $D \in \mathbb{N}$). There exists $\mathbf{K} \in \mathbb{R}^{D \times D}$ s.t.

$$\begin{bmatrix} \mathcal{K}g_1 \\ \vdots \\ \mathcal{K}g_D \end{bmatrix} = \mathbf{K} \begin{bmatrix} g_1 \\ \vdots \\ g_D \end{bmatrix}, \quad (8)$$

if and only if $\text{span}(g_1, \dots, g_D)$ is an invariant subspace under the action of the Koopman operator \mathcal{K} .

Proof. For instance, see [53], in which the non-autonomous setting is adopted but the same argument obviously holds for autonomous systems as well. \square

If (8) holds,

$$\begin{bmatrix} g_1(\chi^+) \\ \vdots \\ g_{N_x}(\chi^+) \end{bmatrix} = \begin{bmatrix} (\mathcal{K}g_1)(\chi) \\ \vdots \\ (\mathcal{K}g_{N_x})(\chi) \end{bmatrix} = \mathbf{K} \begin{bmatrix} g_1(\chi) \\ \vdots \\ g_{N_x}(\chi) \end{bmatrix}, \quad (9)$$

which implies that we can use \mathbf{K} as the parameter \mathbf{A} of model (7) on the assumption that the feature maps g_i are appropriately designed so that (8) holds and \mathbf{K} can be computed in some way. Indeed, with the design of g_i fixed, \mathbf{K} can be easily estimated by EDMD[55].

Furthermore, it has been shown that the approximation \mathbf{K} obtained by EDMD converges to the true Koopman operator in the Strong Operator Topology (SOT)[27]. On several mathematical assumptions, as the number of feature maps g_i and the number of data points used to estimate \mathbf{K} tend to infinity, the EDMD operator converges to \mathcal{K} in SOT. Therefore, it may be judicious in the autonomous setting to add as many feature maps and data points as possible. This will eventually render the EDMD approximation converged to the true Koopman operator, which is sufficient to guarantee an accurate model for most modeling purposes.

2.3 Extending the Koopman Operator Framework to Non-Autonomous Systems

While the Koopman operator framework can be used to form a rigorous basis for linear embedding models in the autonomous setting as seen in the previous section, the non-autonomous setting obstructs some of its useful properties from being true, which brings about several difficulties and challenges to the problem of interest. In this section, we review the Koopman operator formalism for non-autonomous systems. It is then followed by theoretical analyses in the next section, where we show some fundamental limitations of linear embedding models.

To define the Koopman operator for the non-autonomous system (1), we first need to define a set $l(\mathcal{U})$ of infinite sequences of admissible inputs, i.e.,

$$l(\mathcal{U}) := \{\mathbf{U} : \mathbb{Z}_{\geq 0} \rightarrow \mathcal{U} : k \mapsto u_k\} = \{U := (u_0, u_1, \dots) \mid u_k \in \mathcal{U}, k \in \mathbb{Z}_{\geq 0}\}. \quad (10)$$

Also, let \hat{F} be defined as:

$$\hat{F} : \mathcal{X} \times l(\mathcal{U}) \rightarrow \mathcal{X} \times l(\mathcal{U}) : (\chi, U) \mapsto (F(\chi, U(0)), \mathcal{S}U), \quad (11)$$

where \mathcal{S} denotes the shift operator s.t.

$$\mathcal{S}U = \mathcal{S}(u_0, u_1, \dots) := (u_1, u_2, \dots), \quad (12)$$

and $U(0)$ in (11) refers to the first element of $U = (u_0, u_1, \dots)$.

Then, the Koopman operator $\hat{\mathcal{K}}$ for the non-autonomous system (1) is defined as

$$\hat{\mathcal{K}}h = h \circ \hat{F} \Leftrightarrow (\hat{\mathcal{K}}h)(\chi, U) = h(\hat{F}(\chi, U)), \quad h \in \mathcal{H}, \quad (13)$$

where the feature map $h : \mathcal{X} \times l(\mathcal{U}) \rightarrow \mathbb{R}$ is now a function from the direct product $\mathcal{X} \times l(\mathcal{U})$ to the real numbers \mathbb{R} belonging to some function space \mathcal{H} . Note that $l(\mathcal{U})$ needs to be introduced to properly define the domain of h , not \mathcal{U} itself, since if its domain were $\mathcal{X} \times \mathcal{U}$ so that $h : \mathcal{X} \times \mathcal{U} \rightarrow \mathbb{R}$, the definition corresponding to (13) would become $(\hat{\mathcal{K}}h)(\chi, u) = h(F(\chi, u), u^+) = h(\chi^+, u^+)$, which is clearly not well-defined since there exists no successor u^+ of input defined in the dynamics (1).

To avoid this issue, we assume an infinite sequence $U = (u_0, u_1, \dots)$ of inputs so that what $\hat{\mathcal{K}}$ returns after composing two maps can be still well-defined. This also corresponds to the fact that an input *signal* $\mathbf{U} : \mathbb{Z}_{\geq 0} \rightarrow \mathcal{U}$ in (10), which is herein viewed as a function, is assumed to be specified when we introduce the Koopman operator along with the governing equation (1). Note that only specifying a relation between the consecutive two states in time by the difference equation (1) is sufficient to define the discrete-time, non-autonomous dynamics itself. This formal extension to the non-autonomous setting was first developed in [26].

Similar to the previous section, the linear embedding model (2) can be obtained by a finite-dimensional approximation of the Koopman operator $\hat{\mathcal{K}}$ for non-autonomous systems. Consider the following feature maps $h_i : \mathcal{X} \times l(\mathcal{U}) \rightarrow \mathbb{R}$:

$$\begin{bmatrix} h_1(\chi, U) \\ \vdots \\ h_{N_x}(\chi, U) \\ h_{N_x+1}(\chi, U) \\ \vdots \\ h_{N_x+p}(\chi, U) \end{bmatrix} = \begin{bmatrix} g_1(\chi) \\ \vdots \\ g_{N_x}(\chi) \\ U(0) \end{bmatrix}, \quad (14)$$

where $g_i : \mathcal{X} \rightarrow \mathbb{R}$ are some functions from the state space \mathcal{X} into \mathbb{R} .

Proposition 1 also holds in the non-autonomous setting, i.e., it is also true if $g_i \in \mathcal{F}$ and \mathcal{K} are replaced with $h_i \in \mathcal{H}$ and $\hat{\mathcal{K}}$, respectively, as stated in its proof. Suppose $\text{span}(h_1, \dots, h_{N_x+p})$ is an invariant subspace under the action of $\hat{\mathcal{K}}$ so that there exists $\hat{\mathbf{K}} \in \mathbb{R}^{(N_x+p) \times (N_x+p)}$ s.t.

$$\begin{bmatrix} \hat{\mathcal{K}}h_1 \\ \vdots \\ \hat{\mathcal{K}}h_{N_x+p} \end{bmatrix} = \hat{\mathbf{K}} \begin{bmatrix} h_1 \\ \vdots \\ h_{N_x+p} \end{bmatrix}. \quad (15)$$

Also, let χ^+ be the successor that corresponds to $\chi \in \mathcal{X}$ and $U(0) \in \mathcal{U}$. Then, we have

$$\begin{aligned} \begin{bmatrix} g_1(\chi^+) \\ \vdots \\ g_{N_x}(\chi^+) \\ U(1) \end{bmatrix} &= \begin{bmatrix} g_1(F(\chi, U(0))) \\ \vdots \\ g_{N_x}(F(\chi, U(0))) \\ U(1) \end{bmatrix} = \begin{bmatrix} h_1(\hat{F}(\chi, U)) \\ \vdots \\ h_{N_x+p}(\hat{F}(\chi, U)) \end{bmatrix} = \begin{bmatrix} (\hat{\mathcal{K}}h_1)(\chi, U) \\ \vdots \\ (\hat{\mathcal{K}}h_{N_x+p})(\chi, U) \end{bmatrix} \\ &= \hat{\mathbf{K}} \begin{bmatrix} h_1(\chi, U) \\ \vdots \\ h_{N_x+p}(\chi, U) \end{bmatrix} = \hat{\mathbf{K}} \begin{bmatrix} g_1(\chi) \\ \vdots \\ g_{N_x}(\chi) \\ U(0) \end{bmatrix}. \end{aligned} \quad (16)$$

If we define $[\mathbf{A} \ \mathbf{B}] \in \mathbb{R}^{N_x \times (N_x+p)}$ as the upper N_x rows of $\hat{\mathbf{K}}$, the first N_x equations of (16) read:

$$\begin{bmatrix} g_1(\chi^+) \\ \vdots \\ g_{N_x}(\chi^+) \end{bmatrix} = [\mathbf{A} \ \mathbf{B}] \begin{bmatrix} g_1(\chi) \\ \vdots \\ g_{N_x}(\chi) \\ U(0) \end{bmatrix} = \mathbf{A} \begin{bmatrix} g_1(\chi) \\ \vdots \\ g_{N_x}(\chi) \end{bmatrix} + \mathbf{B}U(0), \quad (17)$$

which justifies the use of model (2) for the nonlinear dynamics (1) if the assumptions made so far are satisfied. To estimate $[\mathbf{A} \ \mathbf{B}]$, one can also use EDMD with pre-specified feature maps g_i similar to

the autonomous case[26, 44]. Specifically, given a data set $\{(\chi_i, u_i, y_i) \mid y_i = F(\chi_i, u_i), \chi_i \in \mathcal{X}, u_i \in \mathcal{U}, i = 1, \dots, M\}$, EDMD solves a linear regression problem that minimizes the sum of squared errors over the data points:

$$\min_{[\mathbf{A} \ \mathbf{B}]} \sum_{i=1}^M \left\| \begin{bmatrix} g_1(y_i) \\ \vdots \\ g_{N_x}(y_i) \end{bmatrix} - \left(\mathbf{A} \begin{bmatrix} g_1(\chi_i) \\ \vdots \\ g_{N_x}(\chi_i) \end{bmatrix} + \mathbf{B}u_i \right) \right\|_2^2, \quad (18)$$

which results in the following least square solution:

$$\begin{aligned} [\mathbf{A} \ \mathbf{B}] &= \begin{bmatrix} g_1(y_1) & \cdots & g_1(y_M) \\ \vdots & \ddots & \vdots \\ g_{N_x}(y_1) & \cdots & g_{N_x}(y_M) \end{bmatrix} \begin{bmatrix} g_1(\chi_1) & \cdots & g_1(\chi_M) \\ \vdots & \ddots & \vdots \\ g_{N_x}(\chi_1) & \cdots & g_{N_x}(\chi_M) \\ u_1 & \cdots & u_M \end{bmatrix}^\top \\ &\times \left(\begin{bmatrix} g_1(\chi_1) & \cdots & g_1(\chi_M) \\ \vdots & \ddots & \vdots \\ g_{N_x}(\chi_1) & \cdots & g_{N_x}(\chi_M) \\ u_1 & \cdots & u_M \end{bmatrix} \begin{bmatrix} g_1(\chi_1) & \cdots & g_1(\chi_M) \\ \vdots & \ddots & \vdots \\ g_{N_x}(\chi_1) & \cdots & g_{N_x}(\chi_M) \\ u_1 & \cdots & u_M \end{bmatrix}^\top \right)^\dagger, \quad (19) \end{aligned}$$

where \dagger denotes the Moore-Penrose pseudo inverse.

2.4 Fundamental Limitations of Linear Embedding Models for Non-Autonomous Dynamics

2.4.1 On the Convergence Property of EDMD for Non-Autonomous Systems

While linear embedding models for both autonomous and non-autonomous settings can be associated with the Koopman operator formalism as seen in Sections 2.2 and 2.3, it is known that the convergence property of EDMD that holds for autonomous systems is no longer true in the non-autonomous setting[26]. One of the assumptions required for the convergence property to be true is that the feature maps span an orthonormal basis of the L_2 space as the number of them tends to infinity. However, it is not satisfied in the non-autonomous setting we adopt in this paper, where the feature maps $h_i : \mathcal{X} \times l(\mathcal{U}) \rightarrow \mathbb{R}$ are defined as in (14). Indeed, only the first component of the infinite sequence U appears in (14) and they obviously cannot form any basis of $L_2(\mathcal{X} \times l(\mathcal{U}))$ even if we increase the number of the first N_x feature maps g_i .

A possible way to circumvent this issue is relaxing the specific model structure that the model dynamics is strictly linear w.r.t. u so that the term $\mathbf{B}u$ or $\mathbf{B}U(0)$ in the model representations will be replaced with a general nonlinear function from $l(\mathcal{U})$ to \mathbb{R}^{N_x} . In fact, if the unknown dynamics can be assumed to be a control-affine Ordinary Differential Equation (ODE), it may be beneficial to consider a bilinear model representation by making use of the Koopman canonical transform[50] and an associated bilinearization of the original control-affine dynamics using Koopman generators[17].

However, retaining the strictly linear model dynamics w.r.t. the input u is obviously a quite advantageous factor that allows for the use of well-developed linear systems theories to control unknown nonlinear dynamics as seen in Section 2.1. Therefore, while preserving this linear structure to realize linear controller designs for possibly nonlinear dynamics, we aim to develop a data-driven modeling method that can achieve reasonable approximations of the true dynamics even without the existence of a convergence property. Note that, in contrast to our main focus on the data-driven

modeling aspect, several works also deal with the inevitable modeling error due to this no convergence property and the data-driven nature of EDMD from the controller design perspective[59, 49, 54] (see Section 1 for details).

Neural networks are adopted in the proposed method to learn the feature maps g_i from data, which has been proven to be a promising strategy for Koopman data-driven methods among many other modeling frameworks[42, 51, 30, 58, 40, 19, 20, 57, 53]. Compared to EDMD, in which the feature maps g_i need to be specified by the user, learning a model with g_i characterized by neural networks allows for greater expressivity of the models. On the other hand, it is noted that the neural network training is reduced to a high dimensional non-convex optimization and one may have difficulty training the model properly, e.g., the learning result can easily suffer from overfitting if data is not collected in an appropriate way or the optimization is terminated at an undesired local minimum before the loss function reaches a sufficiently low value. Therefore, the use of neural networks does not necessarily resolve the issues about the modeling error on its own.

2.4.2 Necessary Condition for the Model to Achieve Zero Modeling Error

As another fundamental limitation of the linear embedding models for non-autonomous systems, we provide a necessary condition for the model to achieve precisely zero modeling error. Henceforth, we assume that the model is of the form (3), which includes the state $\chi \in \mathbb{R}^n$ itself as its first n feature maps. Note that this is primarily for the sake of model simplicity and most statements given in this paper can be also true for its generalized representation (2). We define the modeling error $\mathcal{E}(\chi, u)$ at $\chi \in \mathcal{X}$ and $u \in \mathcal{U}$ by

$$\mathcal{E}(\chi, u) := \left\| \begin{bmatrix} \chi^+ \\ g_{n+1}(\chi^+) \\ \vdots \\ g_{N_x}(\chi^+) \end{bmatrix} - \left(\mathbf{A} \begin{bmatrix} \chi \\ g_{n+1}(\chi) \\ \vdots \\ g_{N_x}(\chi) \end{bmatrix} + \mathbf{B}u \right) \right\|_2 \quad (\chi^+ = F(\chi, u)), \quad (20)$$

which is a point-wise error at (χ, u) measured in the embedded space. This represents the accuracy of the model as a finite-dimensional approximation of the Koopman operator. Specifically, we can have $\mathcal{E}(\chi, u) = 0$ for $\forall \chi, u$ if and only if the feature maps g_i span an invariant subspace under the action of the Koopman operator. Also, it reflects the model performance when applied to control applications since $\mathcal{E}(\chi, u) = 0$ is implicitly assumed when controllers are designed for the virtual LTI system (3).

On the other hand, the state predictive accuracy is dictated by the state prediction error $\mathcal{E}_{\text{state}}(\chi, u)$, which is defined as follows:

$$\mathcal{E}_{\text{state}}(\chi, u) := \left\| \chi^+ - \underbrace{\begin{bmatrix} I_n & 0 \end{bmatrix}}_{\text{decoder}} \left(\mathbf{A} \begin{bmatrix} \chi \\ g_{n+1}(\chi) \\ \vdots \\ g_{N_x}(\chi) \end{bmatrix} + \mathbf{B}u \right) \right\|_2. \quad (21)$$

Since $\mathcal{E}(\chi, u) = 0$ implies $\mathcal{E}_{\text{state}}(\chi, u) = 0$, we focus on conditions for $\mathcal{E}(\chi, u) = 0$ in this section. An equivalent condition for $\mathcal{E}_{\text{state}}(\chi, u) = 0$ to be true is provided in [53] along with related discussions.

Noticing that individual components of the embedded state $[\chi^\top \ g_{n+1}(\chi) \ \cdots \ g_{N_x}(\chi)]^\top$ are mutually dependent through the state χ , a necessary condition to eliminate the modeling error $\mathcal{E}(\chi, u)$ is stated as follows.

Proposition 2. For arbitrary $\chi \in \mathcal{X}$ and $u \in \mathcal{U}$, the following is a necessary condition for $\mathcal{E}(\chi, u) = 0$ to hold:

$$\mathbf{A} \begin{bmatrix} \chi \\ g_{n+1}(\chi) \\ \vdots \\ g_{N_x}(\chi) \end{bmatrix} + \mathbf{B}u \in \mathcal{M}, \quad (22)$$

where \mathcal{M} is a set on which the embedded state is defined, i.e.,

$$\mathcal{M} := \left\{ v = [v_1 \cdots v_{N_x}]^\top \in \mathbb{R}^{N_x} \mid \chi \in \mathcal{X}, \left\{ \begin{array}{l} [v_1 \cdots v_n]^\top = \chi \\ v_i = g_i(\chi) (i = n+1, \dots, N_x) \end{array} \right\} \right\}. \quad (23)$$

Proposition 2 states that for the model (3) to achieve $\mathcal{E}(\chi, u) = 0$, it is necessary that its trajectory is constrained on the set \mathcal{M} . Note that the output of the model, or the r.h.s. of (3), may not be on \mathcal{M} in practice due to the incompleteness of the model.

This necessary condition can be written in another form, which suggests the difficulty of achieving $\mathcal{E}(\chi, u) = 0$ for various input values, as shown in the following proposition.

Proposition 3. Suppose that there exist a model of the form (3), $\chi_0 \in \mathcal{X}$, and $u_0 \in \mathcal{U}$ s.t. (22) holds at χ_0 and u_0 , i.e., for χ_0 and u_0 , there exists $\hat{\chi}_0 \in \mathcal{X}$ s.t.

$$\mathbf{A} \begin{bmatrix} \chi_0 \\ g_{n+1}(\chi_0) \\ \vdots \\ g_{N_x}(\chi_0) \end{bmatrix} + \mathbf{B}u_0 = \begin{bmatrix} \hat{\chi}_0 \\ g_{n+1}(\hat{\chi}_0) \\ \vdots \\ g_{N_x}(\hat{\chi}_0) \end{bmatrix}. \quad (24)$$

The following is an equivalent condition for (22) to be also true at χ_0 and any other $u \in \mathcal{U}$: For any $u \in \mathcal{U}$, there exists $\chi \in \mathcal{X}$ s.t.

$$\mathbf{B}\Delta u = \begin{bmatrix} \chi - \hat{\chi}_0 \\ g_{n+1}(\chi) - g_{n+1}(\hat{\chi}_0) \\ \vdots \\ g_{N_x}(\chi) - g_{N_x}(\hat{\chi}_0) \end{bmatrix}, \quad (25)$$

where $\Delta u := u - u_0$.

Proof. Suppose that (24) holds for some $\hat{\chi}_0, \chi_0 \in \mathcal{X}$, and $u_0 \in \mathcal{U}$. If (22) is true for χ_0 and an

arbitrary $u \in \mathcal{U}$, there exists $\chi \in \mathcal{X}$ s.t.

$$\begin{bmatrix} \chi \\ g_{n+1}(\chi) \\ \vdots \\ g_{N_x}(\chi) \end{bmatrix} = \mathbf{A} \begin{bmatrix} \chi_0 \\ g_{n+1}(\chi_0) \\ \vdots \\ g_{N_x}(\chi_0) \end{bmatrix} + \mathbf{B}u_0 + \mathbf{B}\Delta u, \quad (26)$$

where $\Delta u := u - u_0$. Subtracting (24) from the above equation yields (25).

Conversely, if there exists $\chi \in \mathcal{X}$ s.t. (25) is true for an arbitrary $u \in \mathcal{U}$, we have

$$\begin{aligned} (25) \Leftrightarrow \mathbf{B}u - \mathbf{B}u_0 + \begin{bmatrix} \hat{\chi}_0 \\ g_{n+1}(\hat{\chi}_0) \\ \vdots \\ g_{N_x}(\hat{\chi}_0) \end{bmatrix} &= \begin{bmatrix} \chi \\ g_{n+1}(\chi) \\ \vdots \\ g_{N_x}(\chi) \end{bmatrix}, \\ \Leftrightarrow \mathbf{A} \begin{bmatrix} \chi_0 \\ g_{n+1}(\chi_0) \\ \vdots \\ g_{N_x}(\chi_0) \end{bmatrix} + \mathbf{B}u - \left(\mathbf{A} \begin{bmatrix} \chi_0 \\ g_{n+1}(\chi_0) \\ \vdots \\ g_{N_x}(\chi_0) \end{bmatrix} + \mathbf{B}u_0 \right) + \begin{bmatrix} \hat{\chi}_0 \\ g_{n+1}(\hat{\chi}_0) \\ \vdots \\ g_{N_x}(\hat{\chi}_0) \end{bmatrix} &= \begin{bmatrix} \chi \\ g_{n+1}(\chi) \\ \vdots \\ g_{N_x}(\chi) \end{bmatrix}, \\ \Leftrightarrow \mathbf{A} \begin{bmatrix} \chi_0 \\ g_{n+1}(\chi_0) \\ \vdots \\ g_{N_x}(\chi_0) \end{bmatrix} + \mathbf{B}u &= \begin{bmatrix} \chi \\ g_{n+1}(\chi) \\ \vdots \\ g_{N_x}(\chi) \end{bmatrix}, \quad (\because (24)) \end{aligned}$$

which implies that (22) holds for χ_0 and u since $\chi \in \mathcal{X}$. \square

In Proposition 3, suppose $\mathbf{B} \neq 0$ and consider the model dynamics at some point $\chi_0 \in \mathcal{X}$. Even if there exists a model for which the necessary condition (22) holds at χ_0 and some input u_0 , it is in general difficult to be true at χ_0 and a different input u_1 s.t. $\mathbf{B}u_0 \neq \mathbf{B}u_1$. Indeed, satisfying (25) for all $u \in \mathcal{U}$ is equivalent to the linear subspace $\text{range}(\mathbf{B})$ being a tangent space at every point of \mathcal{M} . Considering that g_i needs to be nonlinear to capture the nonlinearity of the original dynamics (1), satisfying (25) for various inputs while including sufficient complexity or nonlinearity in the model through the design of g_i is not likely to be possible in practice, which can be even seen in the following simple example.

Example 1. For one-dimensional nonlinear dynamics with a scalar input given by:

$$\chi^+ = \sin \chi + u, \quad \chi \in \mathbb{R}, \quad u \in [0, \pi], \quad (27)$$

consider the following model of the form (3):

$$\begin{bmatrix} \chi^+ \\ \sin \chi^+ \end{bmatrix} \approx \mathbf{A} \begin{bmatrix} \chi \\ \sin \chi \end{bmatrix} + \underbrace{\begin{bmatrix} 1 \\ 0 \end{bmatrix}}_{=\mathbf{B}} u, \quad (28)$$

where $\mathbf{A} \in \mathbb{R}^{2 \times 2}$ can be arbitrary for the purpose of this example. Note that this model includes a single feature map $g_2(\chi) = \sin \chi$, which can realize the perfect state prediction, i.e., if the first row

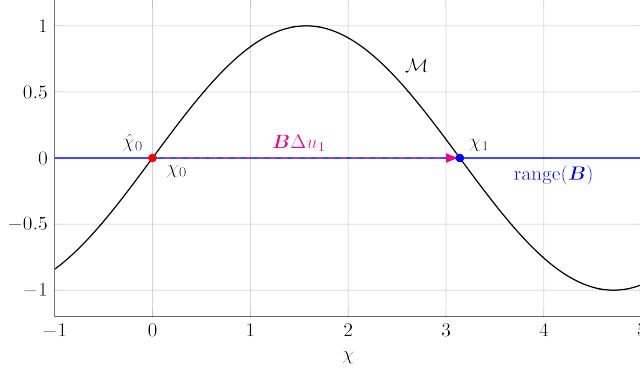


Fig. 2: Embedded space \mathbb{R}^2 associated with the model (28).

Table 1: Modeling errors $\mathcal{E}(\chi_0, u)$ of model (28).

u	$0(=u_0)$	0.5	1.0	1.5	2.0	2.5	$\pi(=u_1)$
$\mathcal{E}(\chi_0, u)$	0	0.479	0.841	0.997	0.909	0.598	0

of \mathbf{A} is $[0 \ 1]$, the first component of the model's output, which is equivalent to its state prediction, becomes $\sin \chi + u$.

At the origin $\chi_0 := 0$ of the state space, this model satisfies the necessary condition given by Proposition 2, or equivalently (24), with the input $u_0 := 0$ since there exists a state $\hat{\chi}_0 := 0$, which satisfies the following:

$$\left(\mathbf{A} \begin{bmatrix} \chi_0 \\ \sin \chi_0 \end{bmatrix} + \mathbf{B}u_0 \right) = \mathbf{A} \begin{bmatrix} 0 \\ 0 \end{bmatrix} + \mathbf{B} \cdot 0 = \begin{bmatrix} 0 \\ 0 \end{bmatrix} \left(= \begin{bmatrix} \hat{\chi}_0 \\ \sin \hat{\chi}_0 \end{bmatrix} \right). \quad (29)$$

Then, by inspecting Fig. 2 or finding roots of the following equation:

$$\sin \chi = 0, \quad (30)$$

we obtain $\chi_1 := \pi$, which satisfies (25) since there exists $u_1 := \pi$ s.t. $\Delta u_1 := u_1 - u_0$ and

$$(\mathbf{B}\Delta u_1) = \begin{bmatrix} 1 \\ 0 \end{bmatrix} \pi = \begin{bmatrix} \pi - 0 \\ 0 - 0 \end{bmatrix} \left(= \begin{bmatrix} \chi_1 - \hat{\chi}_0 \\ \sin \chi_1 - \sin \hat{\chi}_0 \end{bmatrix} \right). \quad (31)$$

Obviously, $u_0 = 0$ and $u_1 = \pi$ are the only inputs u s.t. $u \in [0, \pi]$ and they satisfy (25). Therefore, at the reference state χ_0 , the model (28) can satisfy the necessary condition (22) for $\mathcal{E}(\chi_0, u) = 0$ to be true only if the input u is either $u = u_0$ or $u = u_1$.

As a numerical evaluation, modeling errors at χ_0 and various inputs are listed in Table 1. As expected from Proposition 3, the cases with $u = u_0$ and $u = u_1$ achieve zero modeling errors whereas other input values result in non-zero errors. These errors can be also computed analytically in this example as

$$\mathcal{E}(\chi_0, u) = \left\| \begin{bmatrix} \chi^+ \\ \sin \chi^+ \end{bmatrix} - \mathbf{A} \begin{bmatrix} \chi_0 \\ \sin \chi_0 \end{bmatrix} - \begin{bmatrix} 1 \\ 0 \end{bmatrix} u \right\|_2 = \left\| \begin{bmatrix} u \\ \sin u \end{bmatrix} - \begin{bmatrix} u \\ 0 \end{bmatrix} \right\|_2 = |\sin u|, \quad (32)$$

which becomes 0 only if we choose $u = 0, \pi$, within the admissible set $[0, \pi]$.

This example implies difficulty of deploying the linear embedding model (3) such that it remains accurate across a wide range of operating regimes of dynamics. For instance, if the model (28) is to be used to design a feedback controller represented by:

$$u = \mathbf{Q} \begin{bmatrix} \chi \\ \sin \chi \end{bmatrix}, \quad \mathbf{Q} \in \mathbb{R}^{1 \times 2}, \quad (33)$$

the input u will vary continuously w.r.t. χ and the controller performance may be deteriorated due to the modeling error whenever $u \neq u_0, u_1$, as seen in Table 1 or (32). Note that this analysis based on Proposition 3 is not even related to the Koopman operator formalism and is only concerned with the model structure itself.

The discussions provided in this section imply that even if the model is quite expressive, e.g., with the use of neural networks, and its optimal model parameters minimizing the loss function are obtained in the actual training process, the performance of the model can still suffer from the fundamental limitation as shown in Proposition 3. Indeed, it may be possible that the modeling error $\mathcal{E}(\chi, u)$ is not negligible for a wide range of state/input values due to this limitation.

This observation, combined with the model’s lack of convergence discussed in Section 2.4.1, suggests that learning linear embedding models for non-autonomous dynamics is challenging. In this paper, we propose extending the EDMD-type structure of the model parameters $[\mathbf{A} \ \mathbf{B}]$ by introducing the oblique projection in the context of linear operator-learning in a Hilbert space. This effectively imposes a new type of constraint on $[\mathbf{A} \ \mathbf{B}]$ through the use of test functions that can be viewed as additional degrees of freedom in the training process. As a result, both the accuracy and the generalizability of the model are expected to be improved even in the presence of the fundamental limitations of linear embedding models discussed in this section.

3 Linear Embedding Models with Oblique Projection

In this section, we derive the proposed model architecture, starting from a weak formulation obtained by characterization of the action of a general linear operator w.r.t. a finite dimensional subspace of a Hilbert space. We focus on a finite dimensional linear operator that appears in the weak formulation, which will be utilized to obtain the operator that governs the dynamics of the proposed linear embedding model. It is numerically estimated through a finite data approximation and used as the parameters $[\mathbf{A} \ \mathbf{B}]$.

3.1 Weak Formulation for Characterizing a Linear Operator

Let $\mathcal{L} : H \rightarrow H$ be a linear operator acting on a Hilbert space H and consider the problem of finding \mathcal{L} given data obtained from simulations or experiments. If H is a space of functions defined on a set \mathbb{X} , the data takes the form $\{g(x_i), (\mathcal{L}g)(x_i) \mid x_i \in \mathbb{X}, g : \mathbb{X} \rightarrow \mathbb{R} \in H\}$.

Since it is quite challenging to find a possibly infinite-dimensional \mathcal{L} directly, we instead consider its restriction to some finite-dimensional subspace W , i.e., $\mathcal{L}|_W : W \rightarrow H : g \mapsto \mathcal{L}g$. If W is invariant under the action of \mathcal{L} , there exists a unique matrix representation of $\mathcal{L}|_W$ given a basis of W . Therefore, we aim to find a subspace W , or equivalently its basis, such that it spans an invariant subspace. While this strategy itself does not provide a solution to the problem of finding \mathcal{L} , only obtaining a matrix representation of its restriction to a finite-dimensional invariant subspace is in

fact enough for many engineering applications that utilize the linear operator-learning framework to realize prediction, analyses, and control of dynamical systems.

Given a finite-dimensional subspace $W \subset H$, consider a direct decomposition of H s.t.

$$H = W \oplus E, \quad (34)$$

where E is a complementary subspace. This decomposition is well-defined since we can at least take the orthogonal direct decomposition: $H = W \oplus W^\perp$, whose existence is ensured for a general Hilbert space H . Note that for $\forall g \in W$, $\mathcal{L}|_W g \in H$ may not stay in W ($\mathcal{L}|_W g \in W$ is true if and only if W is an invariant subspace), and it can be decomposed as follows:

$$\mathcal{L}|_W g = Lg + e, \quad (35)$$

where $L : W \rightarrow W$ is an operator that assigns a unique element of W when $\mathcal{L}g$ is decomposed according to (34) and $e \in E$ is the other corresponding unique element of E , respectively.

The second term e may be interpreted as the projection error by considering a (possibly oblique) projection operator $P_{W,E} : H \rightarrow W$, which is defined as:

$$P_{W,E}h := w \text{ for } \forall h \in H, \text{ where } h = w + e, \ w \in W, \ e \in E. \quad (36)$$

It is easily confirmed that $P_{W,E}$ is a linear operator. By definition, the operator L can be represented as

$$L = P_{W,E}\mathcal{L}|_W. \quad (37)$$

Herein, we aim to find this finite dimensional operator L since $\mathcal{L}|_W = L$ if and only if W is an invariant subspace. Let $\{\psi_i\}_{i=1}^N$ be a basis of W , where $N = \dim(W)$. If we take $g = \psi_i$ in (35), there exists a unique element $e_i \in E$ s.t.

$$\mathcal{L}|_W \psi_i = L\psi_i + e_i. \quad (38)$$

Furthermore, $L\psi_i \in W$ can be represented as a linear combination of the basis $\{\psi_i\}_{i=1}^N$, that is, for each $\psi_i \in W$, there exist unique coefficients $l_{ij} \in \mathbb{R}$, $j = 1, \dots, N$, and a unique element $e_i \in E$ s.t.

$$\mathcal{L}|_W \psi_i = \sum_{j=1}^N l_{ij} \psi_j + e_i, \quad i = 1, \dots, N. \quad (39)$$

Note that \mathbf{L}^\top denotes a matrix representation of L , where $\mathbf{L} := (l_{ij}) \in \mathbb{R}^{N \times N}$. A solution to the relaxed problem of finding $\mathcal{L}|_W$ can be reduced to seeking W such that it is invariant under \mathcal{L} and computing a matrix representation \mathbf{L}^\top of L .

To obtain an explicit representation of \mathbf{L}^\top , we introduce a weak formulation: let $\{\varphi_l\}_{l=1}^{\hat{N}}$ be a basis of another finite dimensional subspace $\hat{W} \subset H$ s.t. $\hat{W} = E^\perp$ and take inner products of both sides of (39) with φ_l , $l = 1, \dots, \hat{N}$, so that

$$\begin{aligned} (39) \Rightarrow \langle \mathcal{L}|_W \psi_i, \varphi_l \rangle &= \sum_{j=1}^N l_{ij} \langle \psi_j, \varphi_l \rangle + \langle e_i, \varphi_l \rangle = [l_{i1} \cdots l_{iN}] \begin{bmatrix} \langle \psi_1, \varphi_l \rangle \\ \vdots \\ \langle \psi_N, \varphi_l \rangle \end{bmatrix} + \langle e_i, \varphi_l \rangle, \\ & \quad i = 1, \dots, N, \quad l = 1, \dots, \hat{N}, \\ \Leftrightarrow (\langle \mathcal{L}|_W \psi_i, \varphi_j \rangle) &= \mathbf{L} (\langle \psi_i, \varphi_j \rangle). \end{aligned} \quad (40)$$

Note that the weak formulation (40) is a necessary condition for (39) to hold.

Remark 1. If we choose $E = W^\perp$, i.e., adopt the orthogonal direct decomposition, we have $\hat{W} = W$ and $\varphi_i = \psi_i$ for $\forall i = 1, \dots, N$. Also, if $(\langle \psi_i, \psi_j \rangle)$ is invertible, $\hat{\mathbf{L}} := (\langle \mathcal{L}|_W \psi_i, \psi_j \rangle) (\langle \psi_i, \psi_j \rangle)^{-1}$ gives a necessary condition for $\hat{\mathbf{L}}$ to be a matrix representation of the operator $L = P_{W, W^\perp} \mathcal{L}|_W$. Furthermore, L is in this case an optimal approximation of $\mathcal{L}|_W$ in the following sense:

$$Lg = \operatorname{argmin}_{h \in W} \|\mathcal{L}|_W g - h\|, \quad \forall g \in W. \quad (41)$$

3.2 Finite Data Approximation of L

In practice, it may not be possible to compute the exact values of $\langle \psi_i, \varphi_j \rangle$ or $\langle \mathcal{L}|_W \psi_i, \varphi_j \rangle$ in the weak formulation (40) but one may be able to compute their approximations, which yield a finite data approximation of L , or equivalently \mathbf{L} .

In this section, it is assumed that $H = L_2(\mathbb{X})$, i.e., an L_2 space of functions defined on some set \mathbb{X} . Given a basis $\{\psi_i\}_{i=1}^N$ of the finite dimensional subspace W of H , suppose that the following set of data points is available from either experiments or simulations:

$$\{\boldsymbol{\psi}(x_l), (\mathcal{L}|_W \boldsymbol{\psi})(x_l), \boldsymbol{\varphi}(x_l) \mid x_l \in \mathbb{X}, l = 1, \dots, M\}, \quad (42)$$

where

$$\boldsymbol{\psi}(x_l) := [\psi_1(x_l) \quad \dots \quad \psi_N(x_l)]^\top \in \mathbb{R}^N, \quad (43)$$

$$(\mathcal{L}|_W \boldsymbol{\psi})(x_l) := [(\mathcal{L}|_W \psi_1)(x_l) \quad \dots \quad (\mathcal{L}|_W \psi_N)(x_l)]^\top \in \mathbb{R}^N, \quad (44)$$

$$\boldsymbol{\varphi}(x_l) := [\varphi_1(x_l) \quad \dots \quad \varphi_{\hat{N}}(x_l)]^\top \in \mathbb{R}^{\hat{N}}. \quad (45)$$

If we adopt the empirical measure defined as

$$\mu_M := \frac{1}{M} \sum_{i=1}^M \delta_{x_i}, \quad (46)$$

where δ_{x_i} denotes the Dirac measure at point x_i , we have

$$\langle \psi_i, \varphi_j \rangle_{L_2(\mu_M)} = \int_{\mathbb{X}} \psi_i \varphi_j d\mu_M = \frac{1}{M} \sum_{l=1}^M \psi_i(x_l) \varphi_j(x_l), \quad (47)$$

$$\langle \mathcal{L}|_W \psi_i, \varphi_j \rangle_{L_2(\mu_M)} = \int_{\mathbb{X}} (\mathcal{L}|_W \psi_i) \varphi_j d\mu_M = \frac{1}{M} \sum_{l=1}^M (\mathcal{L}|_W \psi_i)(x_l) \varphi_j(x_l), \quad (48)$$

for $i = 1, \dots, N$ and $j = 1, \dots, \hat{N}$, where the notation $\langle \cdot, \cdot \rangle_{L_2(\mu_M)}$ is used to explicitly indicate that the specific measure (46) is taken. Therefore, the matrices appeared in (40) are in this case reduced to:

$$\langle \psi_i, \varphi_j \rangle_{L_2(\mu_M)} = \frac{1}{M} \sum_{l=1}^M \boldsymbol{\psi}(x_l) \boldsymbol{\varphi}(x_l)^\top, \quad (49)$$

$$\langle (\mathcal{L}|_W \psi_i), \varphi_j \rangle_{L_2(\mu_M)} = \frac{1}{M} \sum_{l=1}^M (\mathcal{L}|_W \boldsymbol{\psi})(x_l) \boldsymbol{\varphi}(x_l)^\top, \quad (50)$$

which can be computed from the data set (42). In the sequel, the notation \mathbf{L}_M is used to refer to the approximated matrix representation of L for which the empirical measure (46) is adopted, i.e.,

$$\begin{aligned} \mathbf{L}_M &:= (\langle \mathcal{L}|_W \psi_i, \varphi_j \rangle_{L_2(\mu_M)}) (\langle \psi_i, \varphi_j \rangle_{L_2(\mu_M)})^\dagger \\ &= \frac{1}{M} \sum_{l=1}^M (\mathcal{L}|_W \boldsymbol{\psi})(x_l) \boldsymbol{\varphi}(x_l)^\top \left\{ \frac{1}{M} \sum_{l=1}^M \boldsymbol{\psi}(x_l) \boldsymbol{\varphi}(x_l)^\top \right\}^\dagger, \end{aligned} \quad (51)$$

where \dagger denotes the Moore-Penrose pseudo inverse. When $N = \hat{N}$ and the matrix $(\langle \psi_i, \varphi_j \rangle_{L_2(\mu_M)})$ is invertible, the pseudo inverse can be replaced with the matrix inverse; otherwise, the pseudo inverse is introduced as the least-square or minimum-norm approximate solution to the problem of finding \mathbf{L} in (40).

Note that the finite-data approximation \mathbf{L}_M may need to be compared with \mathbf{L} derived with the original measure μ , which is supposed to be consistent with actual scenarios in experiments or simulations, e.g., a uniform distribution supported on an interval corresponding to the range of values that can be measured by experimental devices. In general, increasing the number M of data points is advisable to mitigate the discrepancy originating from this finite-data approximation, as seen in the following remark.

Remark 2. Let $\psi_i : \mathbb{X} \rightarrow \mathbb{R}$ and $\varphi_i : \mathbb{X} \rightarrow \mathbb{R}$ be measurable functions for $\forall i$. If $\{x_l\}_{l=1}^M$ in the data set (42) are realizations of independent and identically distributed random variables X_l ($l = 1, \dots, M$), $\psi_i(X_l)$ and $\varphi_i(X_l)$ are also random variables for $\forall l, i$. By the strong law of large numbers, the following holds with probability one:

$$\langle \psi_i, \varphi_j \rangle_{L_2(\mu_M)} \rightarrow \langle \psi_i, \varphi_j \rangle_{L_2(\mu)} \quad (M \rightarrow \infty), \quad (52)$$

where μ denotes a probability measure that corresponds to the probability distribution from which X_l are sampled.

Example 2. The method to compute \mathbf{L}_M described in this section is equivalent to EDMD when \mathcal{L} is a Koopman operator, $\hat{N} = N$, and $\varphi_i = \psi_i$ for $\forall i = 1, \dots, N$. This fact is easily inferred from the following proposition.

Proposition 4. Suppose that $N < M$ and $[\boldsymbol{\psi}(x_1) \ \cdots \ \boldsymbol{\psi}(x_M)] \in \mathbb{R}^{N \times M}$ has full rank. If the orthogonal direct decomposition is adopted in (34) so that $E = W^\perp$, $\hat{N} = N$, and $\varphi_i = \psi_i$ for $\forall i = 1, \dots, N$, the finite data approximation \mathbf{L}_M in (51) is the least-square solution to the problem:

$$\min_{\hat{\mathbf{L}} \in \mathbb{R}^{N \times N}} \sum_{l=1}^M \|(\mathcal{L}|_W \boldsymbol{\psi})(x_l) - \hat{\mathbf{L}} \boldsymbol{\psi}(x_l)\|_2^2. \quad (53)$$

Proof. See Appendix A. □

3.3 Linear Embedding Model Revisited

In this section, we revisit the linear embedding model (3) and derive the same type of model representation from the projection-based linear operator-learning formalism developed in previous sections.

This new perspective enables us to extend the model structure of EDMD by introducing the test functions φ_i into the model parameters $[\mathbf{A} \ \mathbf{B}]$, which are expected to increase the expressivity of the model as well as improve its accuracy and generalizability.

Recall that the unknown non-autonomous dynamics to be modeled was given by

$$\chi^+ = F(\chi, u), \quad \chi \in \mathcal{X} \subseteq \mathbb{R}^n, \quad u \in \mathcal{U} \subseteq \mathbb{R}^p, \quad F : \mathcal{X} \times \mathcal{U} \rightarrow \mathcal{X}, \quad (1)$$

and the space of infinite sequences of admissible inputs was also introduced to define the Koopman operator for this system s.t.

$$l(\mathcal{U}) := \{U : \mathbb{Z}_{\geq 0} \rightarrow \mathcal{U} : k \mapsto u_k\} = \{(u_0, u_1, \dots) \mid u_k \in \mathcal{U}, k \in \mathbb{Z}_{\geq 0}\}. \quad (10)$$

From this point on, we assume $\mathbb{X} = \mathcal{X} \times l(\mathcal{U})$ so that the Hilbert space of interest is defined as $H = L_2(\mathcal{X} \times l(\mathcal{U}))$ and the linear operator \mathcal{L} is the Koopman operator $\hat{\mathcal{K}}$, which was defined in (13).

Similar to (14), if we impose a special structure on the basis functions $\psi_i \in H$ s.t.

$$\psi(\chi, U) = \begin{bmatrix} \psi_1(\chi, U) \\ \vdots \\ \psi_{N_x}(\chi, U) \\ \psi_{N_x+1}(\chi, U) \\ \vdots \\ \psi_{N_x+p}(\chi, U) \end{bmatrix} = \begin{bmatrix} g_1(\chi) \\ \vdots \\ g_{N_x}(\chi) \\ U(0) \end{bmatrix} \in \mathbb{R}^{N_x+p}, \quad (54)$$

where $g_i : \mathcal{X} \rightarrow \mathbb{R}$ are functions from the state-space \mathcal{X} into \mathbb{R} , the action of the Koopman operator \mathcal{L} is characterized as follows:

$$(\mathcal{L}\psi)(\chi, U) = \begin{bmatrix} (\mathcal{L}\psi_1)(\chi, U) \\ \vdots \\ (\mathcal{L}\psi_{N_x})(\chi, U) \\ (\mathcal{L}\psi_{N_x+1})(\chi, U) \\ \vdots \\ (\mathcal{L}\psi_{N_x+p})(\chi, U) \end{bmatrix} = \begin{bmatrix} (\psi_1 \circ \hat{F})(\chi, U) \\ \vdots \\ (\psi_{N_x} \circ \hat{F})(\chi, U) \\ (\psi_{N_x+1} \circ \hat{F})(\chi, U) \\ \vdots \\ (\psi_{N_x+p} \circ \hat{F})(\chi, U) \end{bmatrix} = \begin{bmatrix} g_1(\chi^+) \\ \vdots \\ g_{N_x}(\chi^+) \\ U(1) \end{bmatrix} \quad (\because (13)), \quad (55)$$

where χ^+ denotes the successor of χ and $U(0)$ so that $\chi^+ = F(\chi, U(0))$. The direct decomposition (39) reads

$$\begin{aligned} & \begin{bmatrix} (\mathcal{L}\psi_1)(\chi, U) \\ \vdots \\ (\mathcal{L}\psi_{N_x})(\chi, U) \\ (\mathcal{L}\psi_{N_x+1})(\chi, U) \\ \vdots \\ (\mathcal{L}\psi_{N_x+p})(\chi, U) \end{bmatrix} = \mathbf{L} \begin{bmatrix} \psi_1(\chi, U) \\ \vdots \\ \psi_{N_x}(\chi, U) \\ \psi_{N_x+1}(\chi, U) \\ \vdots \\ \psi_{N_x+p}(\chi, U) \end{bmatrix} + \begin{bmatrix} e_1(\chi, U) \\ \vdots \\ e_{N_x+p}(\chi, U) \end{bmatrix}, \\ \Leftrightarrow & \begin{bmatrix} g_1(\chi^+) \\ \vdots \\ g_{N_x}(\chi^+) \\ U(1) \end{bmatrix} = \mathbf{L} \begin{bmatrix} g_1(\chi) \\ \vdots \\ g_{N_x}(\chi) \\ U(0) \end{bmatrix} + \begin{bmatrix} e_1(\chi, U) \\ \vdots \\ e_{N_x+p}(\chi, U) \end{bmatrix}. \quad (\because (54), (55)) \end{aligned} \quad (56)$$

Letting $[\mathbf{A} \ \mathbf{B}] \in \mathbb{R}^{N_x \times (N_x + p)}$ be the first N_x rows of \mathbf{L} , we have

$$\begin{bmatrix} g_1(\chi^+) \\ \vdots \\ g_{N_x}(\chi^+) \end{bmatrix} = \mathbf{A} \begin{bmatrix} g_1(\chi) \\ \vdots \\ g_{N_x}(\chi) \end{bmatrix} + \mathbf{B}u + \begin{bmatrix} e_1(\chi, u) \\ \vdots \\ e_{N_x}(\chi, u) \end{bmatrix}, \quad (57)$$

where $u := U(0)$. Note that we have $e_i(\chi, U) = e_i(\chi, u)$ in the above equation since only the first element of U depends on the definitions of ψ_i as in (54). If we specify $[g_1(\chi) \cdots g_{N_x}(\chi)]^\top := \chi$, this equation is written as

$$\begin{bmatrix} \chi^+ \\ g_{n+1}(\chi^+) \\ \vdots \\ g_{N_x}(\chi^+) \end{bmatrix} = \mathbf{A} \begin{bmatrix} \chi \\ g_{n+1}(\chi) \\ \vdots \\ g_{N_x}(\chi) \end{bmatrix} + \mathbf{B}u + \begin{bmatrix} e_1(\chi, u) \\ \vdots \\ e_{N_x}(\chi, u) \end{bmatrix}, \quad (58)$$

which corresponds to the linear embedding model (3). Note that while this paper focuses on linear embedding models so that linear control theories can be readily utilized, other approaches such as bilinear models can be also derived by imposing appropriate structure on the basis functions ψ_i .

The error terms are explicitly included in (58) and the model parameters $[\mathbf{A} \ \mathbf{B}]$ have a specific interpretation in this case, i.e., they are realized as (the upper rows of) the transpose \mathbf{L} of a matrix representation of the linear operator L defined in (37). It is also noted that the error terms $e_i(\chi, u)$ are elements of the complementary subspace E introduced in (34).

In the proposed method, the finite data approximation \mathbf{L}_M in (51) is computed to estimate $[\mathbf{A} \ \mathbf{B}]$ in the above equation. Specifically, letting $[\mathbf{A} \ \mathbf{B}]$ denote the first N_x rows of \mathbf{L}_M , we have

$$\begin{aligned} [\mathbf{A} \ \mathbf{B}] &= \frac{1}{M} \sum_{l=1}^M \begin{bmatrix} g_1(y_l) \\ \vdots \\ g_{N_x}(y_l) \end{bmatrix} \begin{bmatrix} \varphi_1(\chi_l, u_l) \\ \vdots \\ \varphi_{\hat{N}}(\chi_l, u_l) \end{bmatrix}^\top \left\{ \frac{1}{M} \sum_{l=1}^M \begin{bmatrix} g_1(\chi_l) \\ \vdots \\ g_{N_x}(\chi_l) \\ u_l \end{bmatrix} \begin{bmatrix} \varphi_1(\chi_l, u_l) \\ \vdots \\ \varphi_{\hat{N}}(\chi_l, u_l) \end{bmatrix}^\top \right\}^\dagger \\ &= \begin{bmatrix} g_1(y_1) & \cdots & g_1(y_M) \\ \vdots & \ddots & \vdots \\ g_{N_x}(y_1) & \cdots & g_{N_x}(y_M) \end{bmatrix} \begin{bmatrix} \varphi_1(\chi_1, u_1) & \cdots & \varphi_1(\chi_M, u_M) \\ \vdots & \ddots & \vdots \\ \varphi_{\hat{N}}(\chi_1, u_1) & \cdots & \varphi_{\hat{N}}(\chi_M, u_M) \end{bmatrix}^\top \\ &\quad \times \left(\begin{bmatrix} g_1(\chi_1) & \cdots & g_1(\chi_M) \\ \vdots & \ddots & \vdots \\ g_{N_x}(\chi_1) & \cdots & g_{N_x}(\chi_M) \\ u_1 & \cdots & u_M \end{bmatrix} \begin{bmatrix} \varphi_1(\chi_1, u_1) & \cdots & \varphi_1(\chi_M, u_M) \\ \vdots & \ddots & \vdots \\ \varphi_{\hat{N}}(\chi_1, u_1) & \cdots & \varphi_{\hat{N}}(\chi_M, u_M) \end{bmatrix}^\top \right)^\dagger. \end{aligned} \quad (59)$$

This can be viewed as an extension of the model parameters $[\mathbf{A} \ \mathbf{B}]$ given by EDMD since substituting $\varphi_i = g_i$ for $\forall i$ with $\hat{N} = N_x$ recovers the EDMD solution (19). Figure 3 shows a schematic of the proposed linear embedding model with oblique projection.

4 Learning Procedures

In this section, problems of learning model parameters are formulated. For the linear embedding model (58), suppose that a data set is given as $\{(\chi_i, u_i, y_i) \mid y_i = F(\chi_i, u_i), i = 1, \dots, M\}$. The data

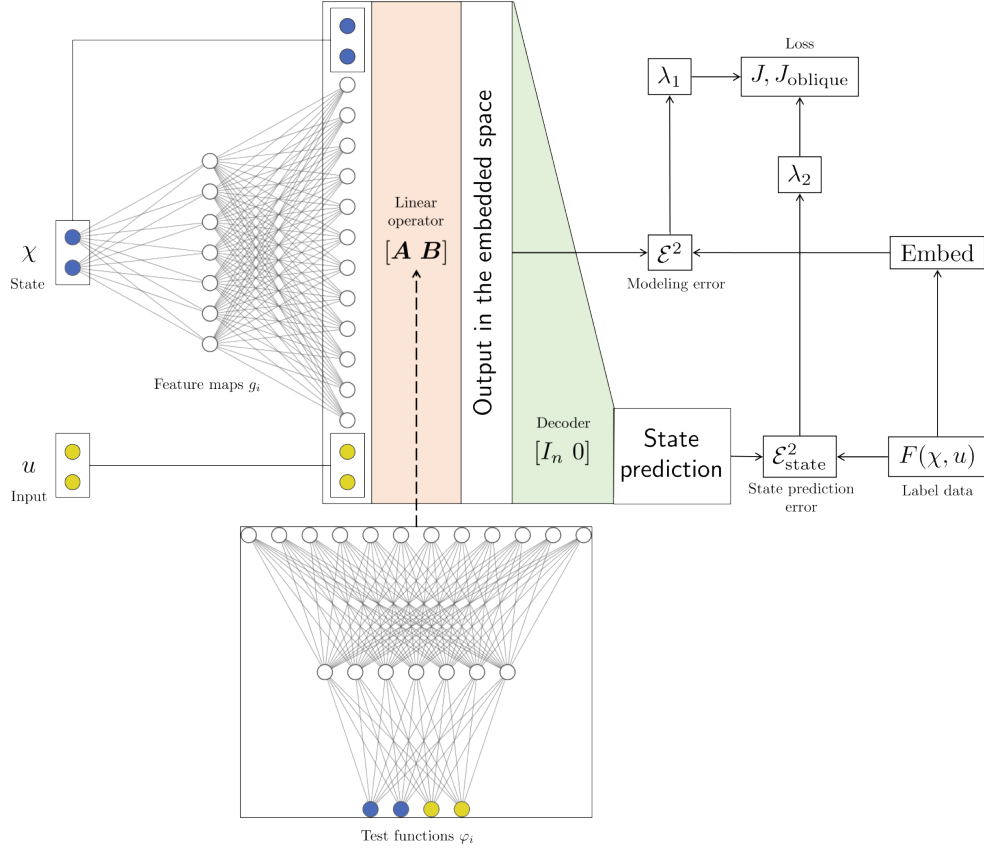


Fig. 3: Architecture of the proposed linear embedding model with oblique projection.

set of the form (42), which was introduced in the context of linear operator learning in Section 3.2, is related to this model as follows:

$$\begin{aligned}
& \{\psi(x_l), (\mathcal{L}_W \psi)(x_l), \varphi(x_l) \mid x_l \in \mathbb{X}, l = 1, \dots, M\} \\
& = \{[\chi_l^\top \ g_{n+1}(\chi_l) \cdots g_{N_x}(\chi_l) \ u_l^\top]^\top, [y_l^\top \ g_{n+1}(y_l) \cdots g_{N_x}(y_l)]^\top, \varphi(\chi_l, u_l) \\
& \quad \mid y_l = F(\chi_l, u_l), l = 1, \dots, M\},
\end{aligned}$$

where the basis functions ψ_i are given by (54) along with a condition $[g_1(\chi) \cdots g_n(\chi)]^\top := \chi$.

Note that the linear operator-learning formulation developed in the previous sections assumes that the functions g_i and φ_i are given. However, the proposed method treats these functions as model parameters to be learned from data. Therefore, computing the approximation \mathbf{L}_M in (51), which corresponds to the model parameters $[A \ B]$, needs to be incorporated into a generalized learning problem where g_i and φ_i are trained on data.

First, noticing the similarity to EDMD as explained in Example 2, we call the procedure to compute (the upper rows of) \mathbf{L}_M the oblique EDMD as follows.

Problem 1. (Oblique EDMD)

Given feature maps $g_i : \mathcal{X} \rightarrow \mathbb{R}$ ($i = 1, \dots, N_x$) and test functions $\varphi_i : \mathcal{X} \times l(\mathcal{U}) \rightarrow \mathbb{R}$ ($i = 1, \dots, \hat{N}$), compute $[\mathbf{A} \ \mathbf{B}]$ in (59), which are then used as the model dynamics parameters of the linear embedding model (58).

The model parameters are initialized by solving the following problem, in which the orthogonal projection is adopted and only the feature maps g_i are the learnable parameters. In the following problem statements, Θ_g denotes neural network parameters that parameterize functions g_i .

Problem 2. (Initialization of model)

Given a data set of the form $\{(\chi_i, u_i, y_i) \mid y_i = F(\chi_i, u_i), i = 1, \dots, M\}$, find Θ_g^0 s.t. $g_i^0(\cdot; \Theta_g^0)$ are a neural network and

$$\Theta_g^0 = \underset{\Theta_g^0 \in \text{Neural network parameters}}{\operatorname{argmin}} J(\Theta_g^0), \quad (60)$$

where

$$\begin{aligned} J(\Theta_g^0) &:= \sum_{i=1}^M \left(\lambda_1 \left\| \begin{bmatrix} y_i \\ g_{n+1}^0(y_i; \Theta_g^0) \\ \vdots \\ g_{N_x}^0(y_i; \Theta_g^0) \end{bmatrix} - \mathbf{A}_0(\Theta_g^0) \begin{bmatrix} \chi_i \\ g_{n+1}^0(\chi_i; \Theta_g^0) \\ \vdots \\ g_{N_x}^0(\chi_i; \Theta_g^0) \end{bmatrix} - \mathbf{B}_0(\Theta_g^0) u_i \right\|_2^2 \right. \\ &\quad \left. + \lambda_2 \left\| y_i - [I \ 0] \left(\mathbf{A}_0(\Theta_g^0) \begin{bmatrix} \chi_i \\ g_{n+1}^0(\chi_i; \Theta_g^0) \\ \vdots \\ g_{N_x}^0(\chi_i; \Theta_g^0) \end{bmatrix} + \mathbf{B}_0(\Theta_g^0) u_i \right) \right\|_2^2 \right) \\ &= \sum_{i=1}^M \{ \lambda_1 \mathcal{E}^2(\chi_i, u_i) + \lambda_2 \mathcal{E}_{\text{state}}^2(\chi_i, u_i) \}, \end{aligned} \quad (61)$$

and $[\mathbf{A}_0(\Theta_g^0) \ \mathbf{B}_0(\Theta_g^0)]$ are computed by Problem 1 with $\varphi_i = g_i^0$ for $\forall i$.

Note that the loss function J is composed of the modeling error and the state prediction error, which were defined in (20) and (21), respectively.

Remark 3. Problem 2 is mathematically equivalent to the implementation of LKIS-DMD [51]. Adding the term involving the input u to the model proposed in [51] and setting $\lambda_1 = 1$, $\lambda_2 = 0$ in Problem 2 yield the same problem.

After the model is initialized by Problem 2, test functions φ_i are also set as learnable parameters and the oblique projection is optimized on different data points.

Problem 3. (Optimizing Oblique Projection)

Suppose a data set $\{(\chi_i, u_i, y_i) \mid y_i = F(\chi_i, u_i), i = 1, \dots, M\}$ is given, which is either a different one from that of Problem 2 or the same one with additional new data points added. Find Θ_g and Θ_φ s.t. $g_i(\cdot; \Theta_g)$ and $\varphi_i(\cdot; \Theta_\varphi)$ are neural networks and

$$\{\Theta_g, \Theta_\varphi\} = \underset{\{\Theta_g, \Theta_\varphi\} \in \text{Neural network parameters}}{\operatorname{argmin}} J_{\text{oblique}}(\Theta_g, \Theta_\varphi), \quad (62)$$

where

$$\begin{aligned} J_{\text{oblique}}(\Theta_g, \Theta_\varphi) &:= \sum_{i=1}^M \left(\lambda_1 \left\| \begin{bmatrix} y_i \\ g_{n+1}(y_i; \Theta_g) \\ \vdots \\ g_{N_x}(y_i; \Theta_g) \end{bmatrix} - \mathbf{A}(\Theta_g, \Theta_\varphi) \begin{bmatrix} \chi_i \\ g_{n+1}(\chi_i; \Theta_g) \\ \vdots \\ g_{N_x}(\chi_i; \Theta_g) \end{bmatrix} - \mathbf{B}(\Theta_g, \Theta_\varphi) u_i \right\|_2^2 \right. \\ &\quad \left. + \lambda_2 \left\| y_i - [I \ 0] \left(\mathbf{A}(\Theta_g, \Theta_\varphi) \begin{bmatrix} \chi_i \\ g_{n+1}(\chi_i; \Theta_g) \\ \vdots \\ g_{N_x}(\chi_i; \Theta_g) \end{bmatrix} + \mathbf{B}(\Theta_g, \Theta_\varphi) u_i \right) \right\|_2^2 \right) \\ &= \sum_{i=1}^M \{ \lambda_1 \mathcal{E}^2(\chi_i, u_i) + \lambda_2 \mathcal{E}_{\text{state}}^2(\chi_i, u_i) \}, \quad (63) \end{aligned}$$

and $[\mathbf{A}(\Theta_g, \Theta_\varphi) \ \mathbf{B}(\Theta_g, \Theta_\varphi)]$ are computed by Problem 1. In the training process, the initial values of the model parameters are set to the result of Problem 2, i.e., $g_i = g_i^0$, $\varphi_i = \varphi_i^0$, $\mathbf{A} = \mathbf{A}_0$, and $\mathbf{B} = \mathbf{B}_0$.

The intent of the two-staged learning procedure consisting of Problem 2 (Initialization by the orthogonal projection) and Problem 3 (Optimization with the oblique projection) is that the model generalizability will be increased by letting the training process have multiple chances to optimize its parameters on different data sets. As seen in Example 2 and Proposition 4, the model derived with the orthogonal projection, which corresponds to the same model structure as EDMD, is already *optimized* being the solution to a linear regression problem. However, it is optimal w.r.t. the summation of 2-norm errors over the given data points and its optimality is not necessarily ensured when different data points are given or other characteristics are adopted as the losses. Thus, the orthogonal projection may not be solely the best choice of model structure, especially from the model's generalizability perspective.

For instance, collecting a sufficient amount of data in a completely unbiased way is difficult in most cases. As a result, the optimized parameters can be varied to a great extent by replacing the data points with different ones. In such a situation, the model may not be generalizable to other regimes of operating points that are not included in the training data.

Based upon these considerations, the proposed method first initializes the model by the orthogonal projection (Problem 2), which ensures the least square type of optimality over the given data, and then optimizes the oblique projection (Problem 3) to allow the training process to have a possible space to increase the generalizability by seeking an optimality on different data points. It is expected that the properties of the initialized model will be altered by introducing additional parameters of the test functions φ_i in Problem 3 and the resulting oblique projection model acquires better performance for a wide range of applications. Similar to optimizations that include regular-

ization terms in the loss function, the proposed modeling method aims to improve the accuracy of the model for an unseen regime of dynamics through the two-stage learning procedure with oblique projections, which may be considered a structural type of constraint imposed on the optimization.

While it is also possible to include other types of errors in the loss function to foster the generalizability further, only the 2-norm errors, $\mathcal{E}(\chi, u)$ and $\mathcal{E}_{\text{state}}(\chi, u)$, are considered in this paper. Determining appropriate characteristics for the loss function is left for future research. Note that the proposed method can also allow the orthogonal projection model by terminating the optimization with $\varphi_i = g_i^0$, in Problem 3. The entire learning procedure is summarized in Algorithm 1. Since we aim to optimize the model on different data points in Problems 2 and 3, the given data set is either divided into two sub data sets or used only partially in Problem 2.

Algorithm 1 Proposed Model Learning

Input: Data set $\mathcal{D} = \{(\chi^+, \chi, u) \mid \chi^+ = F(\chi, u)\}$

Output: Linear embedding model parameters: a linear operator $[\mathbf{A} \ \mathbf{B}]$ and feature maps g_i

- 1: Split \mathcal{D} into sub data sets \mathcal{D}_1 and \mathcal{D}_2 , or extract a part of \mathcal{D} so that $\mathcal{D}_1 \subset \mathcal{D}$ and define $\mathcal{D}_2 := \mathcal{D} \setminus \mathcal{D}_1$
 - 2: Initialize the model on \mathcal{D}_1 by solving Problem 2
 - 3: Train the model on \mathcal{D}_2 by solving Problem 3
-

The use of oblique projections in Problem 3 is expected to alter the properties of the initial model obtained by Problem 2, in a manner comparable to that observed in more straightforward scenarios, e.g., the stability of oblique projection-based models for linear dynamics can be investigated (therefore, can be altered in the model development process) in the context of intrusive reduced-order modeling[46]. The following example showcases a situation where the use of oblique projections plays an important role when the target dynamics possesses the property of non-normality.

Example 3. Consider a two-dimensional nonlinear dynamics $\chi^+ = F(\chi, u)$ given by:

$$\begin{bmatrix} \chi_1^+ \\ \chi_2^+ \end{bmatrix} = \begin{bmatrix} 0.5 & a \\ b & 0.2 \end{bmatrix} \begin{bmatrix} \chi_1 \\ \chi_2 \end{bmatrix} + \begin{bmatrix} \cos \chi_1 - 1 \\ \cos \chi_2 - 1 \end{bmatrix} + \begin{bmatrix} \frac{1}{2} \\ 0 \end{bmatrix} u, \quad (64)$$

where $a, b \in \mathbb{R}$ are constant values and $\chi = [\chi_1 \ \chi_2]^T \in \mathbb{R}^2$. With no control $u \equiv 0$, the origin $\chi = [0 \ 0]^T$ is a fixed point and the corresponding Jacobian:

$$\frac{\partial F}{\partial \chi}([0 \ 0]^T) = \begin{bmatrix} 0.5 & a \\ b & 0.2 \end{bmatrix}, \quad (65)$$

is normal if and only if $a = b$. Figure 4 shows error contour plots of the modeling error $\mathcal{E}(\chi, u \equiv 0)$ defined in (20), where two cases are compared: 1) linear embedding models are trained without oblique projections (model parameters are learned by only Problem 2) and 2) models are trained with oblique projections (model parameters are learned by the proposed Algorithm 1). Two feature maps are included so that the embedded state of the model becomes four dimensional and four test functions are used for the oblique projection. These two types of models are tested on the target systems (64) with two different sets of parameters: 1) $a = b = 0.3$ (Jacobian is normal) and 2) $a = 0.3, b = -0.3$ (Jacobian is non-normal).

When $a = b = 0.3$, in which case the Jacobian is normal, there is no significant difference irrespective of whether the oblique projections are employed (Fig. 4a). On the other hand, when the Jacobian is non-normal, the model trained without oblique projections results in high modeling errors apart from the training data, whereas the proposed method with oblique projections achieves

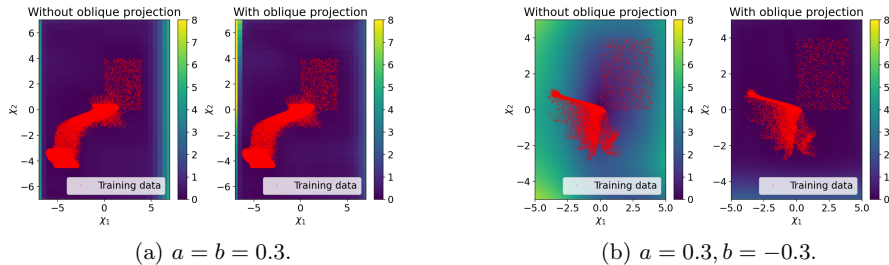


Fig. 4: Comparison of the modeling error $\mathcal{E}(\chi, u \equiv 0)$ between linear embedding models with and without oblique projections.

a quite lower error profile (Fig. 4b). These results imply that the use of oblique projections is necessary in the case of non-normal dynamics of this example to obtain an accurate model. Note that the same training data is used in both training cases with and without oblique projections.

5 Numerical Evaluations

In this section, numerical evaluations are provided to show the effectiveness of the proposed method. In terms of generalizability, a *good* model should be capable of not just capturing the dynamics of the target system accurately, but also be applicable to many different control and decision-making tasks. For instance, MPC is widely employed in the Koopman literature addressing control problems. Long-term predictive accuracy of the model may not be an important factor in this situation since the optimization solved in the MPC procedure is only concerned with the predictions of the model up to a specified finite time horizon and the control objectives may be still achieved even if the model is not quite long-term accurate. On the other hand, long-term predictive accuracy will be essential if the model is to be used for forecasting the system's behavior for a long time. While it may be a practical strategy that one creates a model that is only for a specific task, developing a model that is generalizable to different problems is also of great importance and interest from the modeling perspective. In this paper, we consider the following four tasks to compare the performance and generalizability of different linear embedding models.

State prediction

As one of the most basic tasks of dynamical systems modeling, we consider state prediction. Given an initial condition $\chi_0 \in \mathcal{X}$ and a sequence of inputs $U = (u_0, u_1, \dots)$, $u_i \in \mathcal{U}$, state prediction of a linear embedding model (3) or (58) is implemented according to the following equation:

$$\chi_0^{\text{est}} = \chi_0, \quad \chi_{k+1}^{\text{est}} = [I \ 0] \left(\mathbf{A} \begin{bmatrix} \chi_k^{\text{est}} \\ g_{n+1}(\chi_k^{\text{est}}) \\ \vdots \\ g_{N_x}(\chi_k^{\text{est}}) \end{bmatrix} + \mathbf{B}u_k \right), \quad k = 0, 1, \dots, \quad (66)$$

where $\{\chi_0^{\text{est}}, \chi_1^{\text{est}}, \dots\}$ are the predictions of states. Note that $[I \ 0] \in \mathbb{R}^{n \times N_x}$ is the decoder ω of the model. In this paper, only state prediction with $u_k \equiv 0$ is considered for simplicity. Refer to [53]

for properties of the state prediction (66), including an equivalent condition to achieve zero state prediction error.

Stabilization by LQR

The second task is the stabilization of the unknown dynamics (1) by an LQR designed for the obtained data-driven model. The LQR gain $\mathbf{Q} \in \mathbb{R}^{p \times N_x}$ is computed s.t. the control input is given by $u_k = \mathbf{Q}\xi_k$ and the resulting closed-loop dynamics in \mathbb{R}^{N_x} :

$$\xi_{k+1} = \mathbf{A}\xi_k + \mathbf{B}u_k = (\mathbf{A} + \mathbf{B}\mathbf{Q})\xi_k, \quad \xi_k \in \mathbb{R}^{N_x}, \quad (67)$$

is stabilized at the origin while minimizing the cost function $\sum_{k=0}^{\infty} \xi_k^\top Q_w \xi_k + u_k^\top R_w u_k$, where Q_w and R_w are the weight matrices. Note that the matrices \mathbf{A} and \mathbf{B} in the above equation are given by the data-driven linear embedding model. For instance, they are the solution $[\mathbf{A} \ \mathbf{B}]$ to Problem 3 if the model is obtained by the proposed method. Python Control Systems Library[14] is used to compute the LQR gain.

Reference tracking

We consider reference tracking as the third task. Specifically, a state-feedback controller for a non-zero, steady reference r is designed for a linear embedding model, which is formulated as the following problem[38]:

$$\text{Find } \mathbf{Q}_s, \mathbf{Q}_I \text{ s.t. } \begin{cases} u_k = -\mathbf{Q}_s \xi_k + \mathbf{Q}_I \nu_k \\ \nu_k = \nu_{k-1} + r - y_k \\ y_k = \mathbf{C} \xi_k \\ y_k \rightarrow r \ (k \rightarrow \infty) \end{cases}, \quad (68)$$

where the state $\xi_k \in \mathbb{R}^{N_x}$ is subject to an LTI system $\xi_{k+1} = \mathbf{A}\xi_k + \mathbf{B}u_k$ (\mathbf{A} and \mathbf{B} are given by the data-driven linear embedding model), ν_k denotes a slack variable that corresponds to an integrator of the controller, and \mathbf{C} is an arbitrary matrix with appropriate dimensions that specifies y_k which is expected to follow the reference r , respectively. For more details of the controller design, see [38].

Linear MPC

As the fourth problem, we use linear embedding models for linear MPC, in which we solve the following optimization problem:

$$\begin{aligned} & \min_{u_0, \dots, u_{N_h}} \sum_{k=0}^{N_h-1} \{l(\xi_k, u_k, k) + (u_k - u_{k-1})^\top R(u_k - u_{k-1})\} \\ & \text{subject to: } \begin{cases} \xi_{k+1} = \mathbf{A}\xi_k + \mathbf{B}u_k \\ \text{other constraints on } \xi_k, u_k \end{cases}, \end{aligned} \quad (69)$$

and implement only the first element u_0 at each time. The parameter N_h specifies the finite horizon of the optimization problem and \mathbf{A} and \mathbf{B} in the constraints are given by a data-driven linear embedding model. We set the objective function $l(\xi_k, u_k, k)$ s.t. the specified state will follow a time-varying reference signal. Model predictive control python toolbox[29] is used to produce the results of this paper.

In addition to the generalizability of the model and its performance for individual tasks, the sensitivity of the learning procedure is also of relevance to the numerical evaluation of the method.

The sensitivity analysis of the modeling methods considered in this paper is provided in Section 1 of the Supplementary Material. Also, a discussion on the modeling error $\mathcal{E}(\chi, u)$, or the invariance proximity of the model, is provided in Section 2 of the Supplementary Material.

5.1 Duffing Oscillator

As the first example, we consider the Duffing oscillator, which is given by the following ODE:

$$\ddot{z}(t) = -0.5\dot{z}(t) + z(t) - 4z^3(t) + u(t), \quad (70)$$

where the state $z(t)$ and the input $u(t)$ are continuous variables. With no control $u(t) \equiv 0$, this system has an unstable fixed point $z = 0$ and two stable fixed points $z = \pm 1/2$. We can conceptually consider a first-order time discretization of (70), which is assumed to be the unknown dynamics (1) in the formulations of this paper. The variables $z(t)$ and $\dot{z}(t)$ correspond to the first and second components of $\chi \in \mathbb{R}^2$, respectively.

In the modeling phase, 600 trajectories of states were generated by (70), each of which consists of a single trajectory of 50 discrete-time states sampled at every 0.05 time units, starting from an initial condition $[z(0) \ \dot{z}(0)]^\top$ drawn from the uniform distribution over $[-3, 3]^2 \subset \mathbb{R}^2$. The Runge-Kutta method was used to solve the ODE (70) with the step size of 0.01. Following a data generating strategy suggested in [53], the input data was generated according to $u_k = \cos(\omega_i k \Delta t)$, $\omega_i := 20i$, $i = 0, 1, \dots, 5$, where $\Delta t = 0.05$ denotes the sampling period of data.

In the model learning phase, we trained a proposed model with two feature maps, which yields the embedded state of the form $[\chi^\top \ g_3(\chi) \ g_4(\chi)]^\top$, and four test functions $[\varphi_1(\chi, u) \cdots \varphi_4(\chi, u)]^\top$. Both $[g_3(\chi) \ g_4(\chi)]^\top$ and $[\varphi_1(\chi, u) \cdots \varphi_4(\chi, u)]^\top$ are characterized by a fully connected feed-forward neural network with a single hidden layer consisting of 10 neurons, respectively. The swish function was used as the activation. Problem 2 was solved with half of the data set to initialize the model, which was then followed by solving Problem 3 with the rest of data points added. Model training was implemented in TensorFlow.

For comparison with the proposed method, we also trained two other Koopman-based data-driven models: an EDMD model and a normal neural network model. The EDMD model was obtained by (19) with monomial features up to the third order, which yields the following nine-dimensional embedded state of the model (3):

$$[g_1(\chi) \cdots g_9(\chi)]^\top = [\chi_{(1)} \ \chi_{(2)} \ \chi_{(1)}^2 \ \chi_{(2)}^2 \ \chi_{(1)}\chi_{(2)} \ \chi_{(1)}^3 \ \chi_{(2)}^3 \ \chi_{(1)}^2\chi_{(2)} \ \chi_{(1)}\chi_{(2)}^2]^\top, \quad (71)$$

where we used the notation $[\chi_{(1)} \ \chi_{(2)}]^\top := \chi \in \mathbb{R}^2$. As the normal neural network model, we trained a model by solving Problem 2 only, which is the non-autonomous version of LKIS-DMD[51] as mentioned in Remark 3. It has the same embedding architecture as the proposed model, i.e., two feature maps parameterized by a neural network with the same structure. It is referred to as the normal NN model throughout the rest of the paper. Note that both EDMD and normal NN models were also trained on exactly the same data points as the proposed method. All three models considered here are linear embedding models, but they differ from each other w.r.t. dependency on data or model structures as summarized in Fig. 5.

In the LQR design, we set the weight matrices as

$$Q_w = \begin{bmatrix} Q_{\text{state}} & 0 \\ 0 & 0 \end{bmatrix}, \quad Q_{\text{state}} := \begin{bmatrix} 100 & 0 \\ 0 & 1 \end{bmatrix}, \quad R_w = 1. \quad (72)$$

In the reference tracking problem, we defined $C = [1 \ 0]$ and $r = 1$. In the MPC design, we set the objective function in (69) as follows:

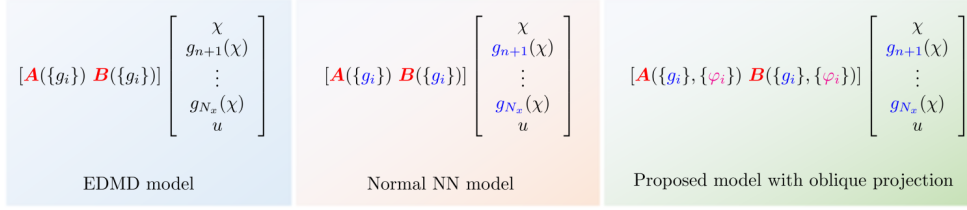


Fig. 5: Comparison of different linear embedding models. Each equation represents the output of the model given the state χ and the input u . Colored variables indicate dependency on data: derivation of \mathbf{A} and \mathbf{B} depends on data in the EDMD model; \mathbf{A} , \mathbf{B} , and $\{g_i\}$ in the normal NN model; \mathbf{A} , \mathbf{B} , $\{g_i\}$, and $\{\varphi_i\}$ in the proposed model. The notation $\mathbf{A}(\{g_i\}, \{\varphi_i\})$ represents the equation defining the matrix \mathbf{A} depends on designs of the feature maps $\{g_i\}$ and the test functions $\{\varphi_i\}$.

$$l(\xi_k, u_k, k) = (\xi_{k,(1)} - r_{\text{MPC}}(k))^2, \quad R = 1, \quad (73)$$

where $\xi_{k,(1)}$ denotes the first component of ξ_k and $r_{\text{MPC}}(k)$ is a time-varying reference signal s.t.

$$r_{\text{MPC}}(k) := \begin{cases} -1 & (k \leq k_c) \\ 1 & (k > k_c) \end{cases}. \quad (74)$$

We set k_c s.t. it corresponds to $t = 10$ in the simulation environment. No additional constraints on ξ_k, u_k were imposed.

The results of the four different tasks are shown in Figs. 6 and 7. First, the EDMD model captures the behavior of the target dynamics quite accurately (Fig. 6a). This is because the Duffing oscillator only has a cubic nonlinearity as in (70) and the embedded state (71) also includes exactly the same nonlinear feature map $\chi_{(1)}^3$. In this case, it is possible to achieve zero state prediction error[53]. A similar result is seen in the error contour plot (Fig. 6d), which shows one-step state prediction errors. On the other hand, the normal NN model fails to obtain accurate state prediction (Figs. 6b and 6e). This is considered as a result of neural network training terminated at an unsatisfactory local minimum for the given data, which showcases the difficulty of training a neural network-based model involving a high-dimensional non-convex optimization as mentioned in Section 2.4.1. Although the normal NN model could be more accurate, one needs to repeat the training process with different initialization of parameters until the learned model shows satisfactory results, which may be prohibitively time-consuming depending on the problem. On the other hand, the proposed model shows quite accurate state predictive accuracy that is comparable to the EDMD model (Figs. 6c and 6f). In Section 3 of the Supplementary Material, a comparison with other general nonlinear classes of models is provided.

The superiority of the proposed method is also observed when the models are deployed in the controller design tasks. In the first application of stabilization by LQR, the EDMD and the normal NN models result in either having a steady state error (normal NN model in Fig. 7b) or altering the closed-loop system unstable (EDMD model in Fig. 7a). On the other hand, the dynamics is successfully stabilized by a controller designed for the proposed model (Fig. 7c). As more quantitative evaluations of stabilization by LQR, Figs. 7d, 7e, and 7f show estimation of basin of attraction, where the responses of the closed-loop dynamics starting from various initial conditions are overlaid in each single plot. The proposed model stabilizes all the given initial conditions, whereas steady-state errors are present with the normal NN model and many simulations diverge with the EDMD model.

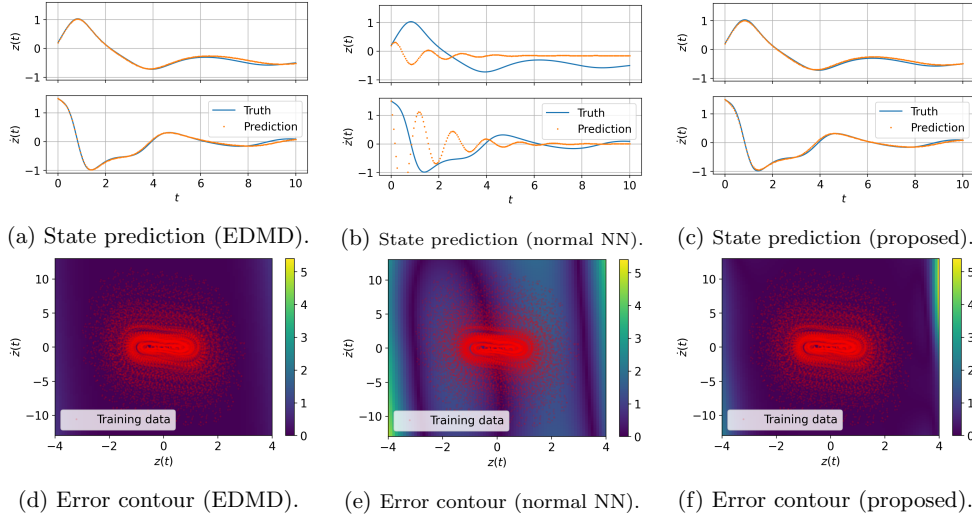


Fig. 6: Results of the Duffing oscillator (state prediction).

For the reference tracking task, the proposed and the normal NN models achieve the control objective (Figs. 7h and 7i) and the EDMD model results in a divergent closed-loop dynamics (Fig. 7g). It is noted that the EDMD model struggles with both stabilization by LQR and the reference tracking although it shows quite accurate state prediction. It is owed to how the modeling error regarding the state prediction differently propagates from that regarding the closed-loop dynamics[53].

Since MPC is only concerned with relatively short-time predictions of the models controlled by the finite horizon of its optimization, none of the three models leads to divergent closed-loop dynamics. Although all the cases do not perfectly track the reference signal, the proposed method has the least amount of steady-state error (Figs. 7j, 7k, and 7l).

5.2 Simple Pendulum

As the second example, we consider the simple pendulum system:

$$\ddot{z}(t) = -\sin z(t) + u(t). \quad (75)$$

The system has fixed points $z = k\pi$ ($k \in \mathbb{Z}$), which are stable for $k = 0, \pm 2, \pm 4, \dots$, and unstable for $k = \pm 1, \pm 3, \dots$. We trained three data-driven models in the same way as the first example of the Duffing oscillator. The conditions and setups for the controller design tasks are also the same as in the first example. The results are shown in Figs. 8 and 9.

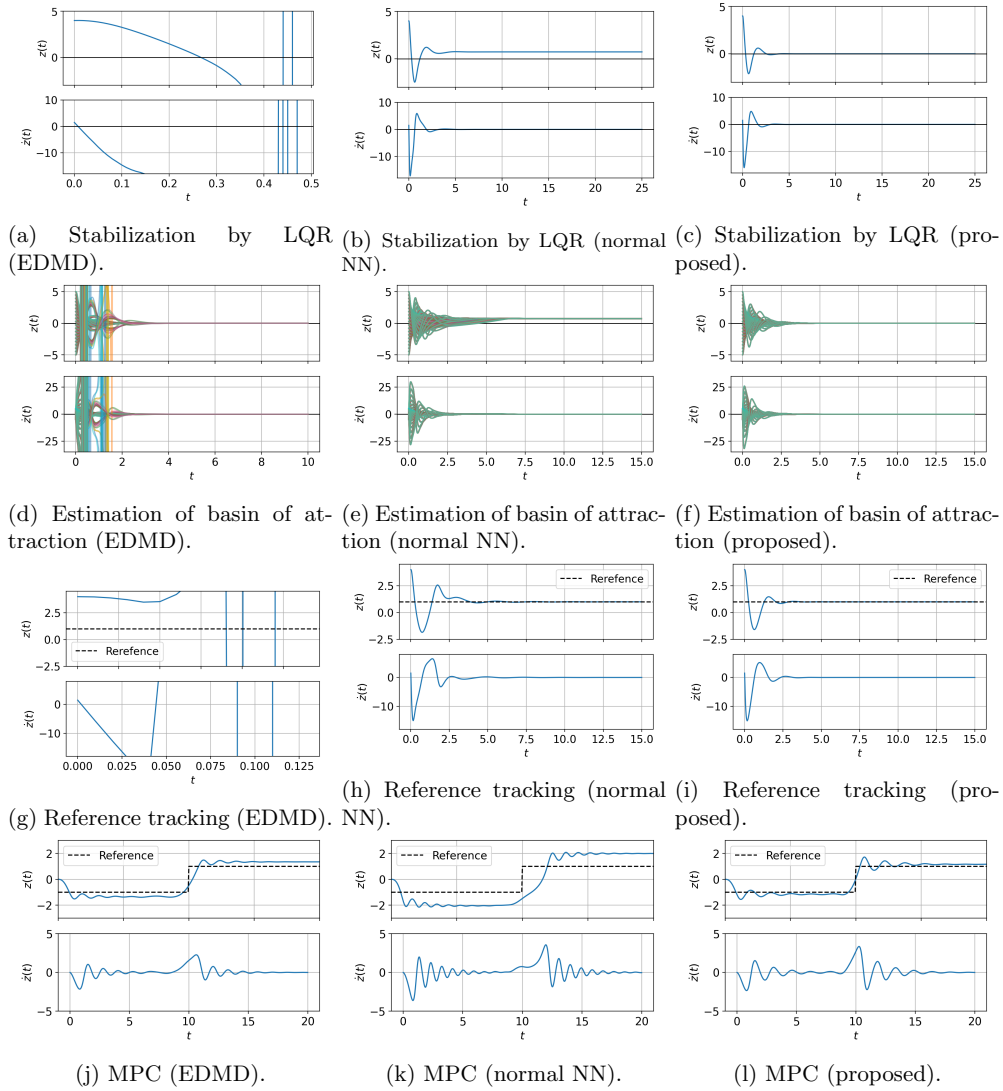


Fig. 7: Results of the Duffing oscillator (control applications).

As opposed to the result in the Duffing oscillator example, the EDMD model fails to predict the state accurately for the simple pendulum (Fig. 8a). This may be inferred from the observation that including more monomial features with higher orders is necessary to reproduce the dynamics near the origin of the state space. It is easily seen by the Taylor series expansion that the dynamics of the simple pendulum may be represented by an infinite number of monomials in the vicinity of local linear approximation at the origin as $\sin z(t) \approx z(t) - z^3(t)/3! + z^5(t)/5! - z^7(t)/7! + \dots$. Therefore, the given embedded state (71) consisting of monomials up to the third order may not be enough to reproduce the original dynamics. However, adding more features to this EDMD model will not be a good strategy for control. Indeed, the embedded state (71) already leads to divergent closed-loop

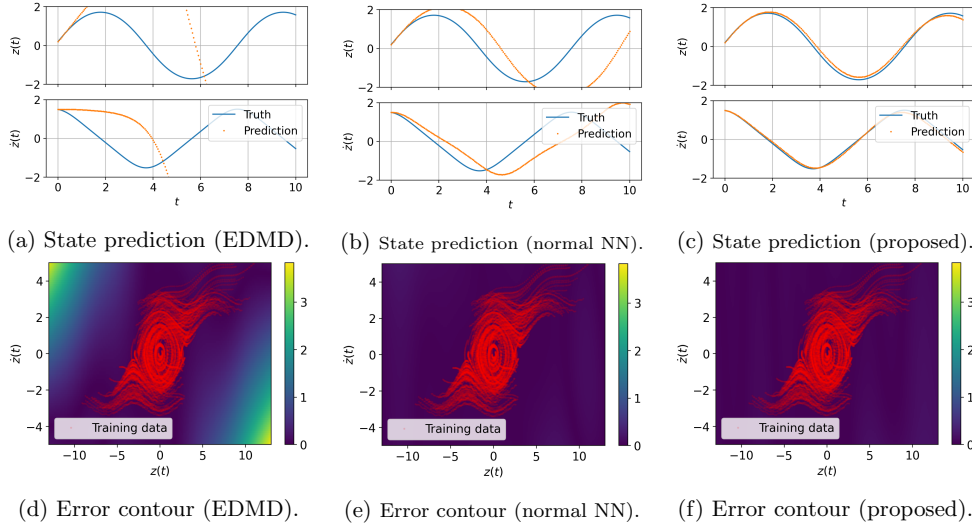


Fig. 8: Results of the simple pendulum (state prediction).

systems in the stabilization by LQR and the reference tracking task (Figs. 9a, 9d, and 9g). This implies that the effect of modeling error $\mathcal{E}(\chi, u)$ in (20) remains quite high leading to unreasonable approximation, and adding more feature maps in this situation may further increase $\|\mathcal{E}(\chi, u)\|$ as suggested in a numerical example in [53].

On the other hand, the other two neural network-based models have reasonable state predictive accuracy. The state predictive error contours of both the normal NN and the proposed models are comparable to each other with quite low error profiles (Fig. 8e and 8f). Also, there are more successful control applications than the EDMD model (Figs. 9b-9l).

In addition to the difference between the EDMD and the neural network-based models, it is also apparent that the proposed model also outperforms the normal NN model in almost all tasks. Whereas the one-step error contours for the normal NN and the proposed models seem quite similar (Figs. 8e and 8f), multi-step state predictive accuracy of the proposed model is more accurate than the normal NN model (Figs. 8b and 8c). Also, the normal NN model only achieves the control objective in the MPC task (Fig. 9k) and the other two control problems result in either a steady-state error (Figs. 9b and 9e) or a divergent simulation (Fig. 9h), whereas the proposed method achieves the control objectives in all tasks (Figs. 9c, 9f, 9i, and 9l).

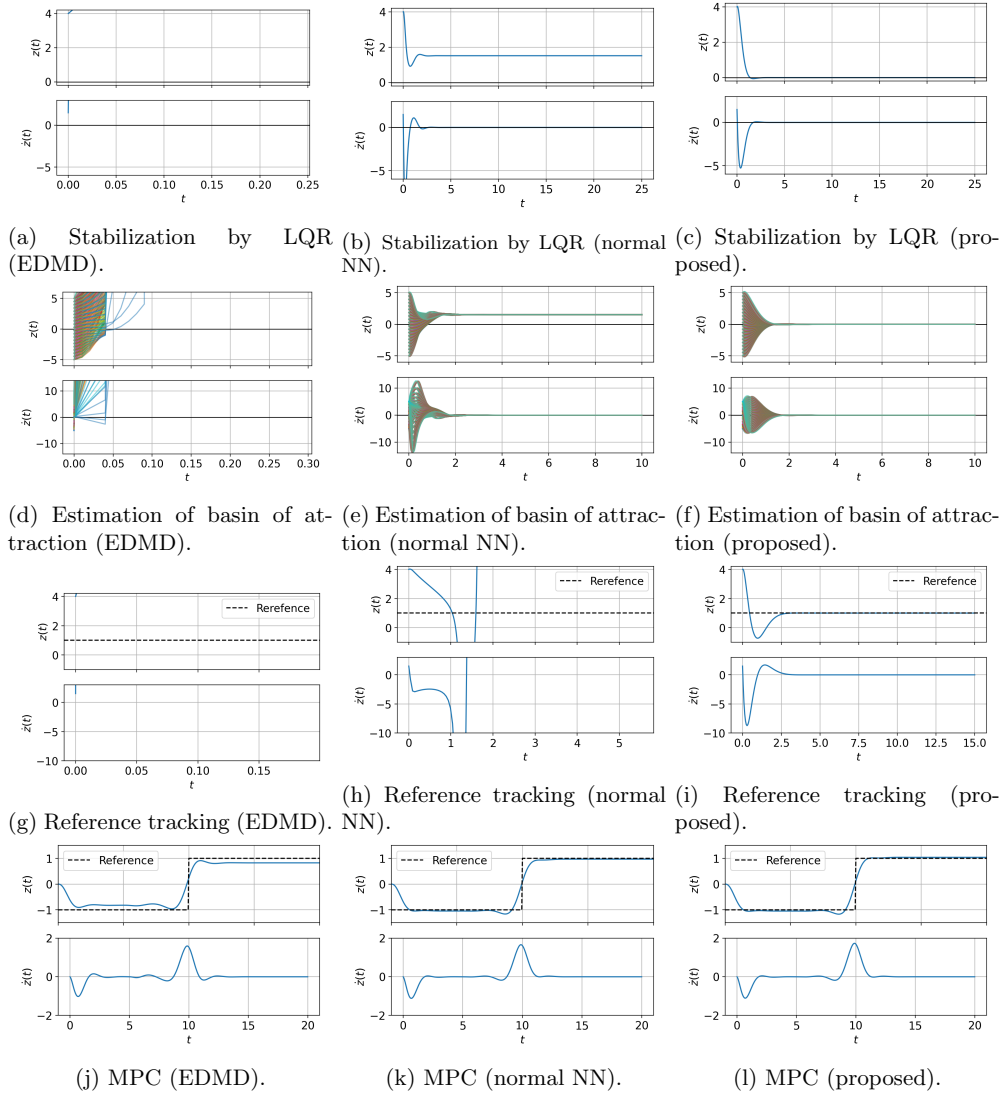


Fig. 9: Results of the simple pendulum (control applications).

5.3 Rotational/Translational Actuator (RTAC)

As the third target system, Rotational/Translational Actuator (RTAC) is considered, which is represented by the following equations[9, 52]:

$$\begin{cases} \dot{z}_1(t) = z_2(t) \\ \dot{z}_2(t) = \frac{-z_1(t) + \epsilon z_4^2(t) \sin z_3(t)}{1 - \epsilon^2 \cos^2 z_3(t)} - \frac{\epsilon \cos z_3(t)}{1 - \epsilon^2 \cos^2 z_3(t)} u(t) \\ \dot{z}_3(t) = z_4(t) \\ \dot{z}_4(t) = \frac{z_1(t) - \epsilon z_4^2(t) \sin z_3(t)}{1 - \epsilon^2 \cos^2 z_3(t)} + \frac{1}{1 - \epsilon^2 \cos^2 z_3(t)} u(t) \end{cases}, \quad (76)$$

where $\epsilon := me/\sqrt{(J + me^2)(M + m)}$. The variables $z_1(t)$, $z_2(t)$, $z_3(t)$, and $z_4(t)$ correspond to the first, second, third, and fourth components of $\chi \in \mathbb{R}^4$, respectively. The system has stable fixed points $[z_1 \ z_2 \ z_3 \ z_4]^\top = [0 \ 0 \ \alpha \ 0]^\top$, where $\alpha \in \mathbb{R}$ is arbitrary.

In this example, an EDMD model was trained with monomial feature maps up to the second order, which yields the 14-dimensional embedded state:

$$[g_1(\chi) \cdots g_{14}(\chi)]^\top = [\chi^\top \ \chi_{(1)}^2 \ \chi_{(2)}^2 \ \chi_{(3)}^2 \ \chi_{(4)}^2 \cdots]^\top, \quad (77)$$

where $[\chi_{(1)} \ \chi_{(2)} \ \chi_{(3)} \ \chi_{(4)}]^\top := \chi$.

For the normal NN and the proposed models, we set the embedded state as follows. Three feature maps are included so that the embedded state is of the form $[\chi \ g_5(\chi) \ g_6(\chi) \ g_7(\chi)]^\top$, where $[g_5(\chi) \ g_6(\chi) \ g_7(\chi)]^\top$ is characterized by a fully connected feed-forward neural network with a single hidden layer consisting of 25 neurons. For the test functions of the proposed method, we adopted a specific structure

$$[\varphi_1(\chi, u) \cdots \varphi_6(\chi, u)]^\top = [\chi^\top \ u \ \varphi_6(\chi)]^\top, \quad (78)$$

with $\varphi_6(\chi)$ be a neural network consisting of a single hidden layer with 10 neurons. We found that imposing the above structure on the design of test functions in (78) leads to not only better performance of the model, but also robust neural network learning as reported in Section 1 of the supplementary material. It suggests that flexible modeling is allowed by having more control over the learning process itself, compared to jointly learning $[\mathbf{A} \ \mathbf{B}]$ and g_i as in [53], where it is difficult to directly regulate the neural network training.

In the LQR design, we set the weight matrices as in (72) with Q_{state} modified as

$$Q_{\text{state}} = \begin{bmatrix} 100 & 0 & 0 & 0 \\ 0 & 1 & 0 & 0 \\ 0 & 0 & 100 & 0 \\ 0 & 0 & 0 & 1 \end{bmatrix}. \quad (79)$$

In the reference tracking problem, we reset $\mathbf{C} = [0 \ 0 \ 1 \ 0]$ with $r = 1$. In the MPC design, we modified the objective function in (73) as $l(\xi, u_k, k) = (\xi_{k,(3)} - r_{\text{MPC}}(k))^2$ so that the third component of the state will track the reference signal.

The results are shown in Figs. 10 and 11. First, the error contour of the EDMD model shows that its one-step state predictive accuracy is not good far from the training data regime (Fig. 10d), whereas the normal NN and the proposed models have lower error profiles across a wide range of operating points (Figs. 10e and 10f). Note that both $z_2(t)$ and $z_4(t)$ are fixed to 0 to visualize the error profiles in two dimensions. On the other hand, multi-step time-series state predictions show different results, where the predictions of $z_3(t)$ and $z_4(t)$ of the proposed model deviate from the true values towards the end of the simulation (Fig. 10c), whereas the other two models output more reasonable state predictions for all the four variables (Figs. 10a and 10b). Noticing that the multi-step predictions start from an initial condition in the training data regime, it implies that the proposed model especially has lower state predictive accuracy on the data points. This is the only result that the performance of the proposed model could not surpass the other two models in the evaluations of this paper.

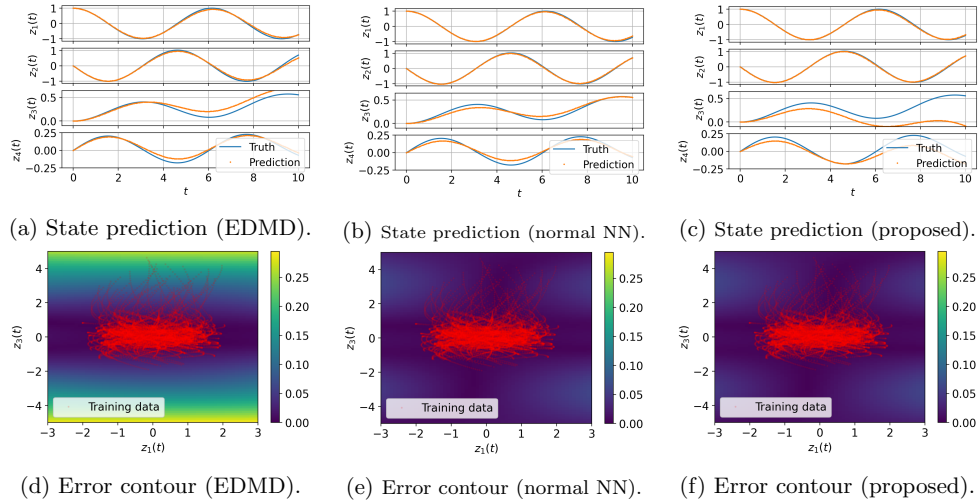


Fig. 10: Results of RTAC (state prediction). In error contour plots, both z_2 and z_4 are fixed to 0.

As for control, the proposed method outperforms the other models in all applications. Except for the MPC task, the EDMD and the normal NN models result in either divergent closed-loop dynamics or undesirable oscillatory behaviors (Figs. 11a, 11d, 11g, 11b, 11e, and 11h). On the other hand, the proposed method enables successful control application in every task (Figs. 11c, 11f, 11i, and 11l), which shows its generalizability to different types of tasks.

6 Conclusion

We propose a new data-driven modeling method for nonlinear, non-autonomous dynamics based on the concept of linear embedding with oblique projection in a Hilbert space. Linear embedding models, which naturally arise as a practical class of models in the Koopman operator framework, have the advantage that linear systems theories can be applied to controller synthesis problems even if the target dynamics is nonlinear. However, there are fundamental limitations regarding the accuracy of the models. In addition to convergence issues associated with Extended Dynamic Mode Decomposition (EDMD) in the non-autonomous setting, we provided a necessary condition for a linear embedding model to achieve zero modeling error as well as subsequent analyses that suggest a fundamental difficulty of obtaining a model that is accurate for a wide range of state/input values.

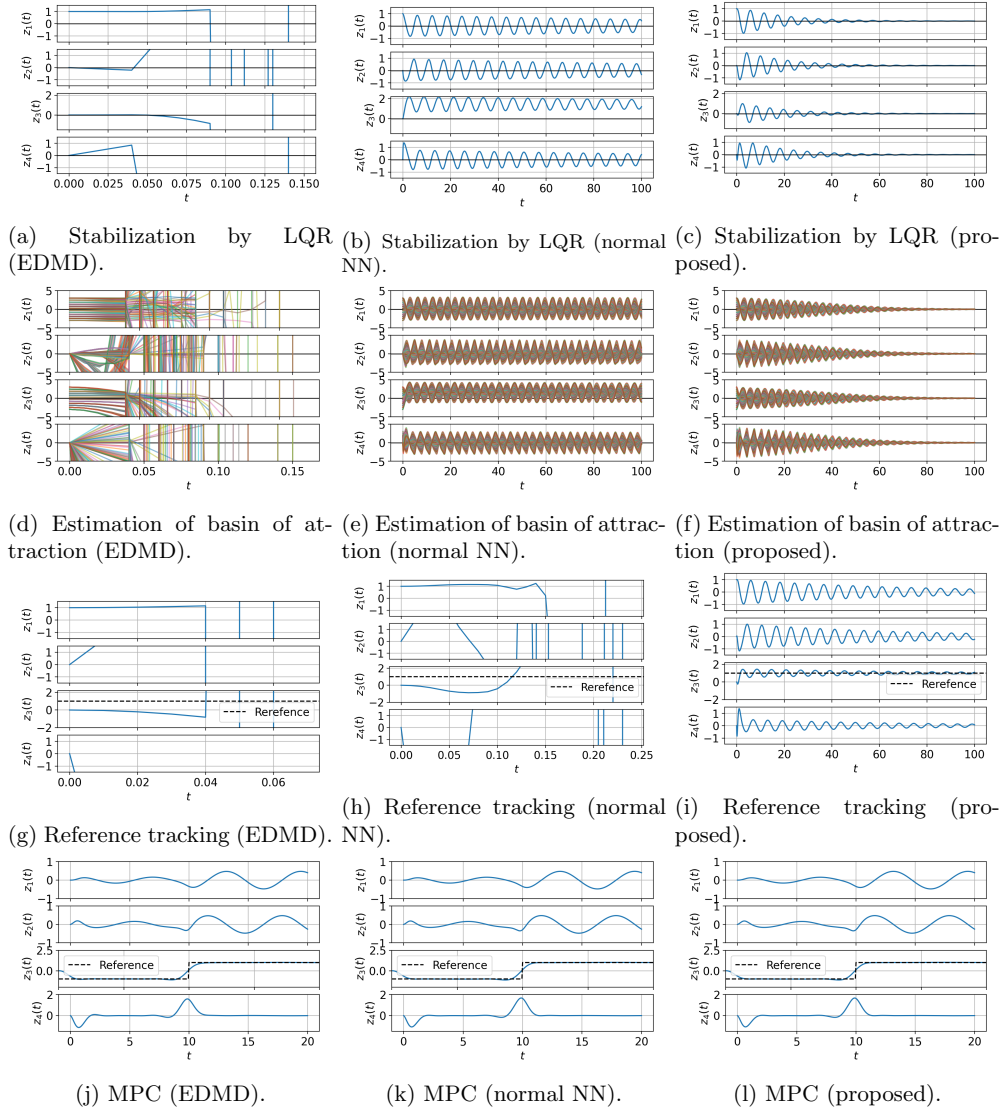


Fig. 11: Results of RTAC (control applications).

This condition reveals a trade-off relation between the expressivity of the model introduced by nonlinear feature maps and the unique model structure of being strictly linear w.r.t. the input to allow the use of linear systems theories for nonlinear dynamics.

To achieve good performance despite these fundamental limitations, we proposed a neural network-based modeling method combined with two-staged learning, which is derived from a weak formulation of projection-based linear operator learning. After initializing a model with orthogonal projection only, which ensures a least square type of optimality w.r.t. given data points, the main training process follows in which test functions that characterize oblique projection are optimized on different

data points along with the feature maps aiming to improve the generalizability of the model so that it can be applicable to many different tasks, including state prediction and various controller design problems. The use of oblique projections is expected to alter the property of the initialized model so that the model accuracy improves for certain dynamics and a simple example was investigated to showcase that the proposed method is effective when the target dynamics possesses the property of non-normality.

To evaluate the proposed method, comprehensive studies were conducted, where four different tasks: state prediction, stabilization by Linear Quadratic Regulator (LQR), reference tracking, and linear Model Predictive Control (MPC) were considered. In each task, we compared the proposed method with other data-driven linear embedding models, targeting three nonlinear dynamics: the Duffing oscillator, the simple pendulum, and the Rotational/Translational Actuator (RTAC). The superiority and effectiveness of the proposed model were confirmed through these various examples and it was shown that it has successfully gained sufficient generalizability.

As a future direction of the research, relaxing the strictly linear structure of the model w.r.t. the input may lead to better accuracy of the model. For instance, bilinear model structures can be advantageous for a wider range of nonlinear dynamics[3]. Also, exploiting prior knowledge about the unknown dynamics may allow for a more rigorous basis for the method from a theoretical perspective. If one restricts the attention to control-affine systems, several theoretical analyses become available, e.g., controllability analysis[17] and finite data error bounds[45, 37]. For the proposed method developed in this paper, it may be also possible to supplement the modeling framework with similar mathematical analyses based on these works. This work considered situations where the dimension of the embedded space of the model is higher than the target dynamics. It may be also useful to explore whether the proposed method can be effectively applied to dynamical systems with large dimensions, in which case the problem is reduced to finding a latent space that can capture the essential properties of the higher-dimensional dynamics. Since the proposed method is only based on the single-step error it may be difficult for the model to learn long-time behaviors. Taking multi-step errors into account may help construct accurate models for these more complex dynamics.

Acknowledgments

This work was funded by APRA-E under the project *SAFARI: Secure Automation for Advanced Reactor Innovation*.

References

- [1] H. ARBABI, M. KORDA, AND I. MEZIĆ, *A data-driven Koopman model predictive control framework for nonlinear partial differential equations*, in 2018 IEEE Conference on Decision and Control (CDC), 2018, pp. 6409–6414.
- [2] P. BENNER, S. GUGERCIN, AND K. WILLCOX, *A survey of projection-based model reduction methods for parametric dynamical systems*, *SIAM Review*, 57 (2015), pp. 483–531.
- [3] D. BRUDER, X. FU, AND R. VASUDEVAN, *Advantages of bilinear Koopman realizations for the modeling and control of systems with unknown dynamics*, *IEEE Robotics and Automation Letters*, 6 (2021), pp. 4369–4376.

- [4] B. W. BRUNTON, L. A. JOHNSON, J. G. OJEMANN, AND J. N. KUTZ, *Extracting spatial-temporal coherent patterns in large-scale neural recordings using dynamic mode decomposition*, *Journal of Neuroscience Methods*, 258 (2016), pp. 1–15.
- [5] S. L. BRUNTON, B. W. BRUNTON, J. L. PROCTOR, AND J. N. KUTZ, *Koopman invariant subspaces and finite linear representations of nonlinear dynamical systems for control*, *PLOS ONE*, 11 (2016), pp. 1–19.
- [6] S. L. BRUNTON, M. BUDIŠIĆ, E. KAISER, AND J. N. KUTZ, *Modern Koopman theory for dynamical systems*, *SIAM Review*, 64 (2022), pp. 229–340.
- [7] S. L. BRUNTON AND J. N. KUTZ, *Data-Driven Science and Engineering: Machine Learning, Dynamical Systems, and Control*, Cambridge University Press, 2019.
- [8] M. BUDIŠIĆ, R. MOHR, AND I. MEZIĆ, *Applied Koopmanism*, *Chaos*, 22 (2012), p. 047510.
- [9] R. BUPP, D. BERNSTEIN, AND V. COPPOLA, *A benchmark problem for nonlinear control design: problem statement, experimental testbed, and passive nonlinear compensation*, in *Proceedings of the 1995 American Control Conference*, vol. 6, 1995, pp. 4363–4367.
- [10] K. CARLBERG, M. BARONE, AND H. ANTIL, *Galerkin v. least-squares Petrov–Galerkin projection in nonlinear model reduction*, *Journal of Computational Physics*, 330 (2017), pp. 693–734.
- [11] M. J. COLBROOK AND A. TOWNSEND, *Rigorous data-driven computation of spectral properties of Koopman operators for dynamical systems*, *Communications on Pure and Applied Mathematics*, 77 (2024), pp. 221–283.
- [12] S. DAS, D. GIANNAKIS, AND J. SLAWINSKA, *Reproducing kernel Hilbert space compactification of unitary evolution groups*, *Applied and Computational Harmonic Analysis*, 54 (2021), pp. 75–136.
- [13] C. FOLKESTAD, Y. CHEN, A. D. AMES, AND J. W. BURDICK, *Data-driven safety-critical control: Synthesizing control barrier functions with Koopman operators*, *IEEE Control Systems Letters*, 5 (2021), pp. 2012–2017.
- [14] S. FULLER, B. GREINER, J. MOORE, R. MURRAY, R. VAN PAASSEN, AND R. YORKE, *The python control systems library (python-control)*, in *60th IEEE Conference on Decision and Control (CDC)*, 2021, pp. 4875–4881.
- [15] M. GEORGESCU AND I. MEZIĆ, *Building energy modeling: A systematic approach to zoning and model reduction using Koopman mode analysis*, *Energy and Buildings*, 86 (2015), pp. 794–802.
- [16] A. GHOLAMI, A. VOSUGHI, AND A. K. SRIVASTAVA, *Denoising and detection of bad data in distribution phasor measurements using filtering, clustering, and Koopman mode analysis*, *IEEE Transactions on Industry Applications*, 58 (2022), pp. 1602–1610.
- [17] D. GOSWAMI AND D. A. PALEY, *Global bilinearization and controllability of control-affine nonlinear systems: A Koopman spectral approach*, in *2017 IEEE 56th Annual Conference on Decision and Control (CDC)*, 2017, pp. 6107–6112.
- [18] D. A. HAGGERTY, M. J. BANKS, P. C. CURTIS, I. MEZIĆ, AND E. W. HAWKES, *Modeling, reduction, and control of a helically actuated inertial soft robotic arm via the Koopman operator*, *arXiv e-prints*, (2020), p. arXiv:2011.07939.

- [19] M. HAN, J. EULER-ROLLE, AND R. K. KATZSCHMANN, *DeSKO: Stability-assured robust control with a deep stochastic Koopman operator*, in The Tenth International Conference on Learning Representations, ICLR, 2022.
- [20] Y. HAN, W. HAO, AND U. VAIDYA, *Deep learning of Koopman representation for control*, in 2020 59th IEEE Conference on Decision and Control (CDC), 2020, pp. 1890–1895.
- [21] C. HUANG, C. R. WENTLAND, K. DURAISAMY, AND C. MERKLE, *Model reduction for multi-scale transport problems using model-form preserving least-squares projections with variable transformation*, Journal of Computational Physics, 448 (2022), p. 110742.
- [22] E. KAISER, J. N. KUTZ, AND S. L. BRUNTON, *Data-driven discovery of Koopman eigenfunctions for control*, Machine Learning: Science and Technology, 2 (2021), p. 035023.
- [23] S. KLUS, P. KOLTAI, AND C. SCHÜTTE, *On the numerical approximation of the Perron-Frobenius and Koopman operator*, Journal of Computational Dynamics, 3 (2016), pp. 51–79.
- [24] S. KLUS, F. NÜSKE, S. PEITZ, J.-H. NIEMANN, C. CLEMENTI, AND C. SCHÜTTE, *Data-driven approximation of the Koopman generator: Model reduction, system identification, and control*, Physica D: Nonlinear Phenomena, 406 (2020), p. 132416.
- [25] B. O. KOOPMAN, *Hamiltonian systems and transformation in Hilbert space*, Proceedings of the National Academy of Sciences, 17 (1931), pp. 315–318.
- [26] M. KORDA AND I. MEZIĆ, *Linear predictors for nonlinear dynamical systems: Koopman operator meets model predictive control*, Automatica, 93 (2018), pp. 149–160.
- [27] M. KORDA AND I. MEZIĆ, *On convergence of extended dynamic mode decomposition to the Koopman operator*, Journal of Nonlinear Science, 28 (2018), pp. 687–710.
- [28] M. KORDA, M. PUTINAR, AND I. MEZIĆ, *Data-driven spectral analysis of the Koopman operator*, Applied and Computational Harmonic Analysis, 48 (2020), pp. 599–629.
- [29] S. LUCIA, A. TĂTULEA-CODREAN, C. SCHOPPMAYER, AND S. ENGELL, *Rapid development of modular and sustainable nonlinear model predictive control solutions*, Control Engineering Practice, 60 (2017), pp. 51–62.
- [30] B. LUSCH, N. J. KUTZ, AND S. L. BRUNTON, *Deep learning for universal linear embeddings of nonlinear dynamics*, Nature Communications, 9 (2018), p. 4950.
- [31] G. MAMAKOUKAS, M. CASTANO, X. TAN, AND T. MURPHEY, *Local Koopman operators for data-driven control of robotic systems*, in Proceedings of the Robotics: Science and Systems, 2019.
- [32] G. MAMAKOUKAS, M. L. CASTANO, X. TAN, AND T. D. MURPHEY, *Derivative-based koopman operators for real-time control of robotic systems*, arXiv e-prints, (2020), arXiv:2010.05778. arXiv:2010.05778.
- [33] W. A. MANZOOR, S. RAWASHDEH, AND A. MOHAMMADI, *Vehicular applications of Koopman operator theory—a survey*, IEEE Access, 11 (2023), pp. 25917–25931.
- [34] A. MAUROY, I. MEZIĆ, AND Y. SUSUKI, *The Koopman Operator in Systems and Control*, Springer International Publishing, 2020.

- [35] I. MEZIĆ, *Spectral properties of dynamical systems, model reduction and decompositions*, Nonlinear Dynamics, 41 (2005), pp. 309–325.
- [36] A. NARASINGAM AND J. S.-I. KWON, *Koopman Lyapunov-based model predictive control of nonlinear chemical process systems*, AIChE Journal, 65 (2019), p. e16743.
- [37] F. NÜSKE, S. PEITZ, F. PHILIPP, M. SCHALLER, AND K. WORTHMANN, *Finite-data error bounds for Koopman-based prediction and control*, Journal of Nonlinear Science, 33 (2022).
- [38] K. OGATA, *Discrete-Time Control Systems*, Prentice Hall, second ed., 1995.
- [39] S. E. OTTO, A. PADOVAN, AND C. W. ROWLEY, *Optimizing Oblique Projections for Nonlinear Systems using Trajectories*, SIAM Journal on Scientific Computing, 44 (2022), pp. A1681–A1702.
- [40] S. E. OTTO AND C. W. ROWLEY, *Linearly recurrent autoencoder networks for learning dynamics*, SIAM Journal on Applied Dynamical Systems, 18 (2019), pp. 558–593.
- [41] S. E. OTTO AND C. W. ROWLEY, *Koopman operators for estimation and control of dynamical systems*, Annual Review of Control, Robotics, and Autonomous Systems, 4 (2021), pp. 59–87.
- [42] S. PAN AND K. DURAISAMY, *Physics-informed probabilistic learning of linear embeddings of nonlinear dynamics with guaranteed stability*, SIAM Journal on Applied Dynamical Systems, 19 (2020), pp. 480–509.
- [43] S. PEITZ AND S. KLUS, *Koopman operator-based model reduction for switched-system control of PDEs*, Automatica, 106 (2019), pp. 184–191.
- [44] J. L. PROCTOR, S. L. BRUNTON, AND J. N. KUTZ, *Dynamic mode decomposition with control*, SIAM Journal on Applied Dynamical Systems, 15 (2016), pp. 142–161.
- [45] M. SCHALLER, K. WORTHMANN, F. PHILIPP, S. PEITZ, AND F. NÜSKE, *Towards reliable data-based optimal and predictive control using extended dmd*, IFAC-PapersOnLine, 56 (2023), pp. 169–174.
- [46] G. SERRE, P. LAFON, X. GLOERFELT, AND C. BAILLY, *Reliable reduced-order models for time-dependent linearized Euler equations*, Journal of Computational Physics, 231 (2012), pp. 5176–5194.
- [47] S. H. SON, H.-K. CHOI, AND J. S.-I. KWON, *Application of offset-free Koopman-based model predictive control to a batch pulp digester*, AIChE Journal, 67 (2021), p. e17301.
- [48] S. H. SON, H.-K. CHOI, J. MOON, AND J. S.-I. KWON, *Hybrid Koopman model predictive control of nonlinear systems using multiple edmd models: An application to a batch pulp digester with feed fluctuation*, Control Engineering Practice, 118 (2022), p. 104956.
- [49] S. H. SON, A. NARASINGAM, AND J. SANG-IL KWON, *Handling plant-model mismatch in Koopman Lyapunov-based model predictive control via offset-free control framework*, arXiv e-prints, (2020), p. arXiv:2010.07239.
- [50] A. SURANA, *Koopman operator based observer synthesis for control-affine nonlinear systems*, in 2016 IEEE 55th Conference on Decision and Control (CDC), 2016, pp. 6492–6499.

- [51] N. TAKEISHI, Y. KAWAHARA, AND T. YAIRI, *Learning Koopman invariant subspaces for dynamic mode decomposition*, Advances in Neural Information Processing Systems, 30 (2017), pp. 1130–1140.
- [52] M. TAVAKOLI, H. D. TAGHIRAD, AND M. ABRISHAMCHIAN, *Identification and robust h_∞ control of the rotational/translational actuator system*, International Journal of Control Automation and Systems, 3 (2005), pp. 387–396.
- [53] D. UCHIDA AND K. DURAISAMY, *Control-aware Learning of Koopman Embedding Models*, arXiv e-prints, (2022), p. arXiv:2209.08637.
- [54] D. UCHIDA, A. YAMASHITA, AND H. ASAMA, *Data-driven Koopman controller synthesis based on the extended \mathcal{H}_2 norm characterization*, IEEE Control Systems Letters, 5 (2021), pp. 1795–1800.
- [55] M. WILLIAMS, I. KEVREKIDIS, AND C. ROWLEY, *A data driven approximation of the Koopman operator: Extending dynamic mode decomposition*, Journal of Nonlinear Science, 25 (2015), pp. 1307–1346.
- [56] M. O. WILLIAMS, M. S. HEMATI, S. T. DAWSON, I. G. KEVREKIDIS, AND C. W. ROWLEY, *Extending data-driven koopman analysis to actuated systems*, IFAC-PapersOnLine, 49 (2016), pp. 704–709.
- [57] Y. XIAO, X. ZHANG, X. XU, X. LIU, AND J. LIU, *Deep neural networks with Koopman operators for modeling and control of autonomous vehicles*, IEEE Transactions on Intelligent Vehicles, 8 (2023), pp. 135–146.
- [58] E. YEUNG, S. KUNDU, AND N. HODAS, *Learning deep neural network representations for Koopman operators of nonlinear dynamical systems*, Proceedings of the 2019 American Control Conference (ACC), (2019), pp. 4832–4839.
- [59] X. ZHANG, W. PAN, R. SCATTOLINI, S. YU, AND X. XU, *Robust tube-based model predictive control with Koopman operators*, Automatica, 137 (2022), p. 110114.

A Proof of Proposition 4

If we define

$$\mathbf{X} := [\boldsymbol{\psi}(x_1) \ \cdots \ \boldsymbol{\psi}(x_M)] \in \mathbb{R}^{N \times M}, \quad \mathbf{Y} := [(\mathcal{L}_{|W}\boldsymbol{\psi})(x_1) \ \cdots \ (\mathcal{L}_{|W}\boldsymbol{\psi})(x_M)] \in \mathbb{R}^{N \times M},$$

the least-square problem (53) can be written as

$$\min_{\hat{\mathbf{L}} \in \mathbb{R}^{N \times N}} \sum_{l=1}^M \|(\mathcal{L}_{|W}\boldsymbol{\psi})(x_l) - \hat{\mathbf{L}}\boldsymbol{\psi}(x_l)\|_2^2 = \min_{\hat{\mathbf{L}} \in \mathbb{R}^{N \times N}} \|\mathbf{Y} - \hat{\mathbf{L}}\mathbf{X}\|_F^2 = \min_{\hat{\mathbf{L}} \in \mathbb{R}^{N \times N}} \|\mathbf{Y}^\top - \mathbf{X}^\top \hat{\mathbf{L}}^\top\|_F^2,$$

which corresponds to solving an over-determined system of equations $\mathbf{X}^\top \hat{\mathbf{L}}^\top = \mathbf{Y}^\top$ with the assumption $N < M$. The unique solution that achieves the least squared error can be obtained by solving the normal equation:

$$\begin{aligned} & \mathbf{X}\mathbf{X}^\top \hat{\mathbf{L}}^\top = \mathbf{X}\mathbf{Y}^\top \\ \Leftrightarrow & \hat{\mathbf{L}}\mathbf{X}\mathbf{X}^\top = \mathbf{Y}\mathbf{X}^\top \\ \Leftrightarrow & \hat{\mathbf{L}} \left\{ \frac{1}{M} \sum_{l=1}^M \boldsymbol{\psi}(x_l)\boldsymbol{\psi}(x_l)^\top \right\} = \frac{1}{M} \sum_{i=1}^M (\mathcal{L}_{|W}\boldsymbol{\psi})(x_i)\boldsymbol{\psi}(x_i)^\top, \end{aligned} \tag{80}$$

which gives (51) with $\psi_i = \varphi_i$ on the assumption that $\mathbf{X}\mathbf{X}^\top$ is invertible, or equivalently \mathbf{X} has full rank.

Supplementary Material for Extracting Koopman Operators for Prediction and Control of Non-linear Dynamics Using Two-stage Learning and Oblique Projections

Daisuke Uchida¹ and Karthik Duraisamy¹

¹Department of Aerospace Engineering, University of Michigan

1 Sensitivity Analysis of the Modeling Methods

In a data-driven modeling procedure, one may need to repeat the model training with or without new data if the learned model does not show satisfactory performance for the given task. For neural network-based models, the training process is often terminated at an undesirable local minimum due to the nature of high-dimensional non-convex optimization. Thus, it may be required to repeat the training process many times to obtain a satisfactory result and the computational cost of model training may be an issue in practice. In this section, the sensitivities of the learning methods are evaluated.

Specifically, in the same settings as in Section 5, we repeated collecting data and training models 10 times as follows:

```

for  $k = 1, \dots, 10$  do
  Collect data to form a data set  $\mathcal{D}_k := \{(y_i, \chi_i, u_i) \mid y_i = F(\chi_i, u_i)\}$ .
  Train an EDMD, a normal NN, and a proposed models using the same data set  $\mathcal{D}_k$ .
end for

```

From the algorithmic perspective, a modeling method is considered robust and reliable if many trials result in high model performance, which implies that one can obtain a model with desirable performance in a small number of trials. Figures S1, S2, and S3 show the results, where the same four tasks as Section 5 are tested on the three dynamical systems and individual results from the 10 trials are overlaid in a single plot for each task.

First, since the EDMD model is obtained by a unique analytical solution to a linear regression problem as in (2.19), its learning results are quite robust, being only influenced by the difference of data points among the 10 trials. However, the result also implies that it is not able to produce desirable results if the choice of feature maps or the quality of data is not appropriate, regardless of the number of trials.

On the other hand, neural network-based models have more chances to obtain better and preferable learning results with the same number of trials, at the expense of more sensitive learning procedures. The results of the normal NN and the proposed models show that some trials can yield successful models even if other learning results completely fail in the given task. Especially, neural

network training initializes its parameter values randomly and this often leads to quite different learning results.

The superiority of the proposed method is also observed in this evaluation. Specifically, in the RTAC case (Fig. S3), only the proposed method is both robust and reliable. The robustness of the proposed method in this example may be attributed to the specific constraint (5.13) imposed on the test functions, which reduces the number of neural network parameters.

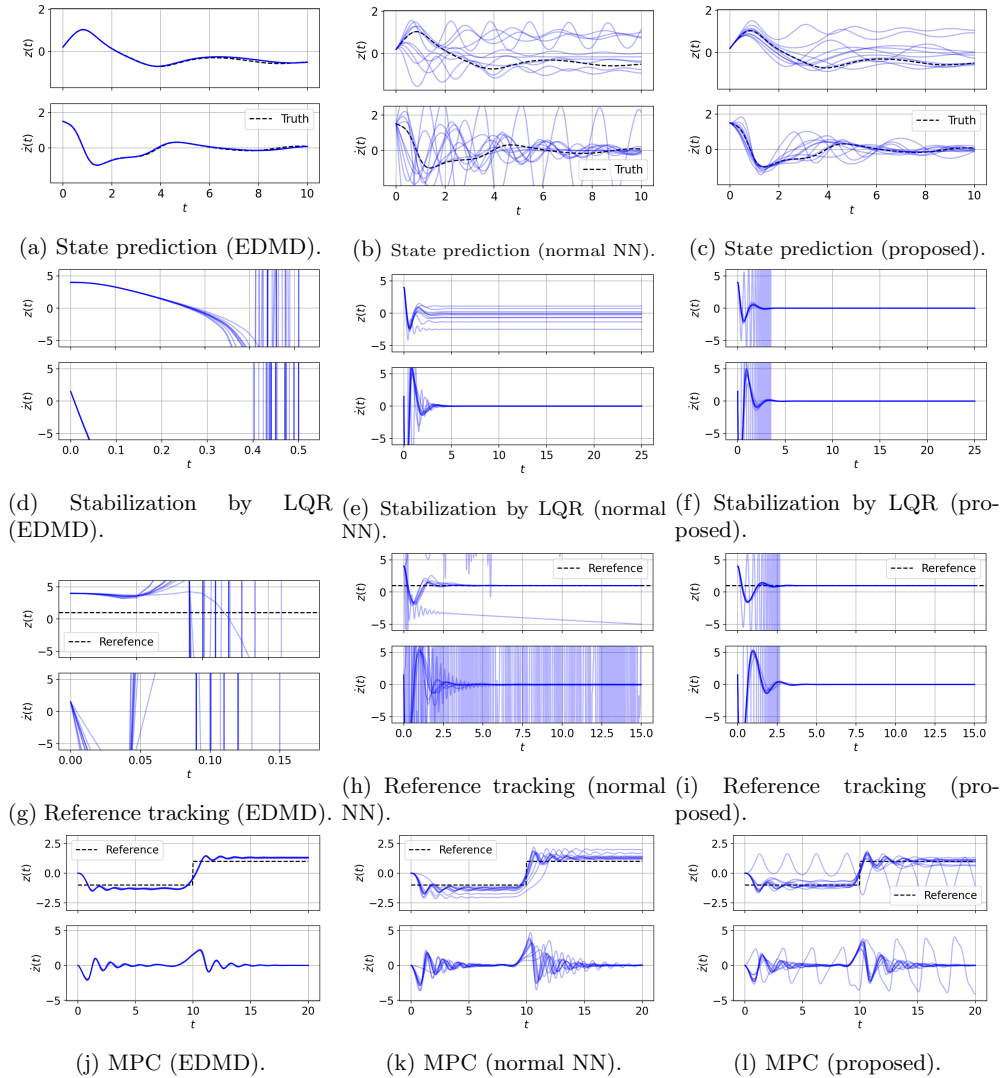


Fig. S1: Sensitivity analysis (Duffing oscillator).

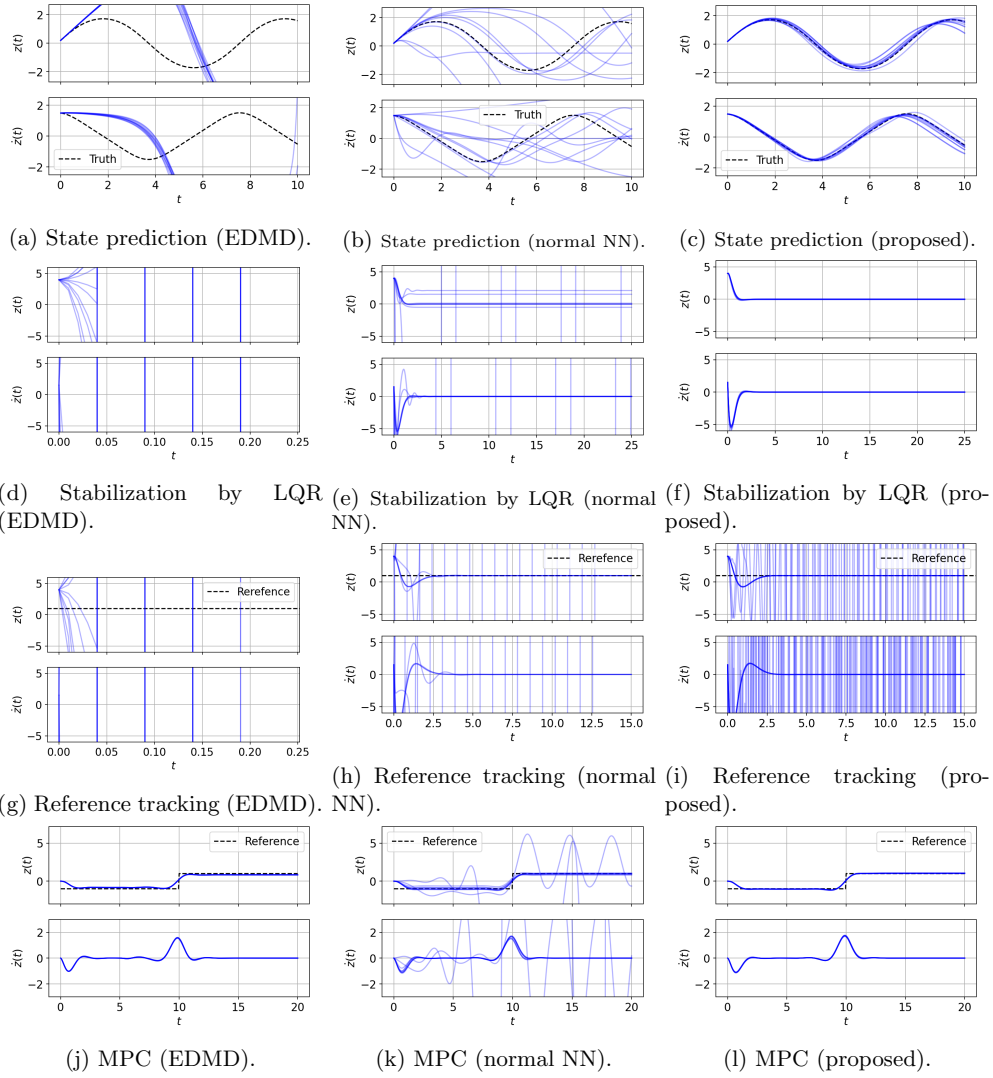


Fig. S2: Sensitivity analysis (simple pendulum).

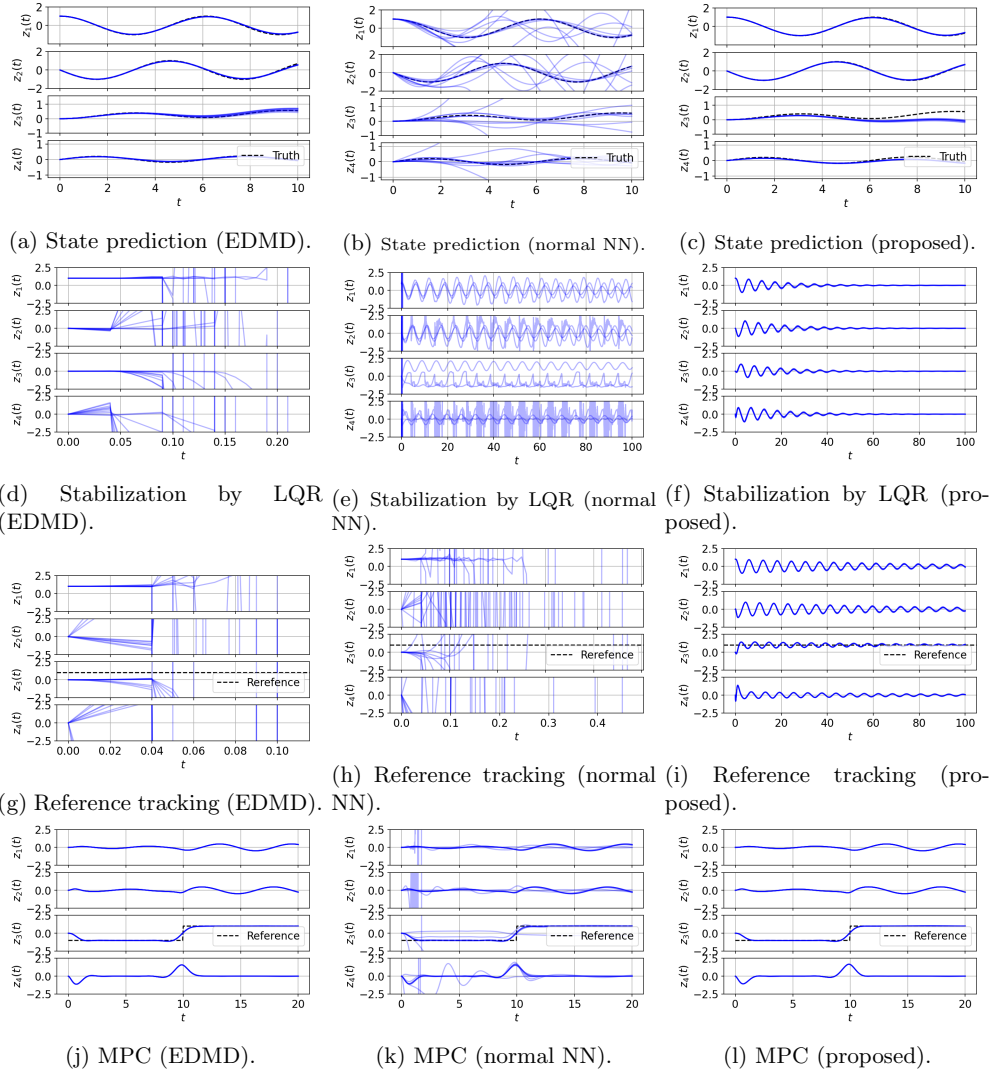


Fig. S3: Sensitivity analysis (RTAC).

2 Invariance Proximity of the Models

While the modeling error (2.20) was introduced in Section 2 for analyzing the model accuracy and it represents the invariance proximity of the linear embedding model, i.e., how close the subspace spanned by the feature maps is to being invariant under the action of the Koopman operator, it is not a suitable metric in practice to measure the model performance with respect to multiple tasks.

Given a state trajectory χ_0, χ_1, \dots of the true dynamics, the invariance proximity of the model can be evaluated by simply evolving a linear embedding model (2.3) as in Algorithm 1.

Algorithm 1 Forecasting by simply evolving the linear embedding model

Require: Initial condition $\chi_0 \in \mathcal{X}$ and input sequence $(u_0, u_1, \dots) \in l(\mathcal{U})$

Ensure: Predicted embedded states $\mathbf{g}_0^{\text{est}}, \mathbf{g}_1^{\text{est}}, \dots$

$$\mathbf{g}_0^{\text{est}} \leftarrow \begin{bmatrix} \chi_0 \\ g_{n+1}(\chi_0) \\ \vdots \\ g_{N_x}(\chi_0) \end{bmatrix}$$

for $k = 1, 2, \dots$ **do**
 $\mathbf{g}_k^{\text{est}} \leftarrow \mathbf{A}\mathbf{g}_{k-1}^{\text{est}} + \mathbf{B}u_{k-1}$
end for

Figure S4 shows the first n components of the predicted embedded states $\mathbf{g}_k^{\text{est}}$ of Algorithm 1. It is apparent from the figure that the predictions by Algorithm 1 differ from the actual state prediction results (Figs. 5, 7, and 9), where the feature maps are re-evaluated at every time step instead of simply evolving the model from the initial condition. Especially, the EDMD and the proposed models show poor forecasting in Fig. S4a whereas both have satisfactory performance in the original state prediction task as in Fig. 6. Similarly, Algorithm 1 yields unstable forecasting for the simple pendulum example (Fig. S4b), whereas only the EDMD model results in the same behavior in the original prediction task (Fig. 8).

Also, the results of the control applications in Section 5 show a diverse range of model performance depending on which controller design and linear embedding model are adopted (Figs. 6, 8, and 10). Therefore, it is unable to measure or infer the performance of individual methods w.r.t. multiple control tasks targeting multiple dynamics by looking at the invariance proximity computed by Algorithm 1. While the invariance proximity is useful to analyze the model accuracy analytically, it is difficult and not stable in practice to measure the generalizability, i.e., the model performance w.r.t. multiple tasks, by Algorithm 1 or only considering the modeling error (2.20).

3 Comparison of State Predictive Accuracy with Nonlinear Models

In this section, a more detailed evaluation of the state predictive accuracy of linear embedding models is provided. Specifically, the state predictions of the linear embedding models trained in Section 5 are compared with nonlinear predictors. The linear embedding models considered in this paper are concerned with the state predictive accuracy by the second term $\lambda_2 \mathcal{E}_{\text{state}}^2(\chi_i, u_i)$ of the loss functions and the invariance proximity as an approximation of the Koopman operator, which corresponds to their first term $\lambda_1 \mathcal{E}^2(\chi_i, u_i)$. On the other hand, general nonlinear predictor models are likely to possess higher accuracy if they are trained with loss functions that only minimize the state prediction

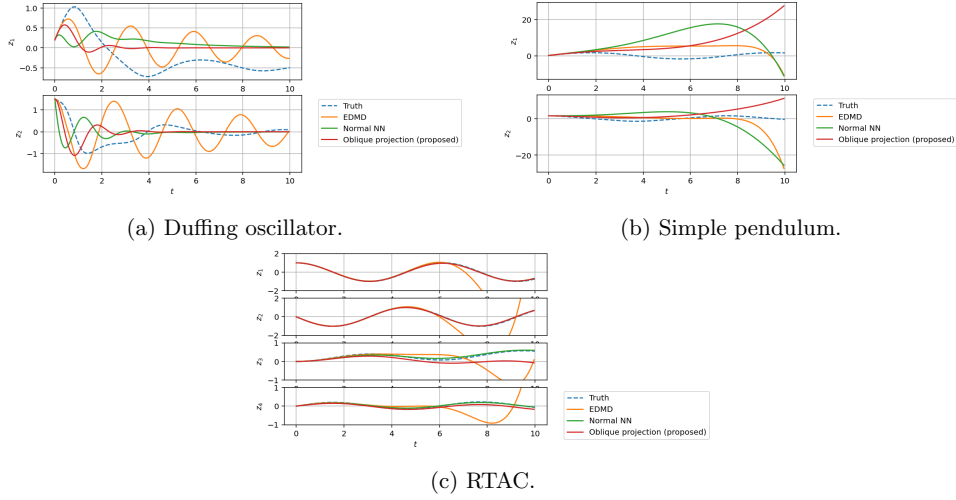


Fig. S4: Forecasting by Algorithm 1.

error. To compare the state predictive accuracy of different types of models, two nonlinear models are considered in this section. Sparse Identification of Nonlinear Dynamical Systems (SINDy)[1, 2] is a modeling method to learn nonlinear predictors that identify functional forms of the target dynamics based on sparse regression. The resulting model equations are linear combinations of candidate dictionaries of feature maps that are pre-specified by the user. As another nonlinear model, a neural network-based predictor is considered, which is a feedforward neural network $F_{NN} : \mathcal{X} \times \mathcal{U} \rightarrow \mathcal{X}$ that directly predicts the state at the next time step given a pair of state and input. Both nonlinear models are trained on exactly the same data set as the linear embedding models in Section 5. For SINDy models, polynomial features are used and a feedforward neural network consisting of two hidden layers with the Rectified Linear Unit (ReLU) activation is used to train the neural network predictor F_{NN} .

Figure S5 shows the comparison of the state predictive accuracy of both the linear embedding models from Section 5 and the two nonlinear predictors. Both the SINDy model and the neural network predictor show good state predictive accuracy in all three examples, which is considered due to the fact that they are general nonlinear predictors trained to only minimize the state prediction error. Also, the proposed model is the only linear embedding model that also performs well in all examples. Normal NN model fails the prediction task for the Duffing oscillator and the simple pendulum (Figs. S5a and S5b) and the EDMD model results in an unstable prediction for the simple pendulum (Fig. S5b). It is observed that the prediction of the proposed model deviates from the truth in the third component $z_3(t)$ in the example of RTAC (Fig. S5c). It is considered as a result of the trade-off relation between the robustness or reliability of the training procedure, which is stated in Section 1 and Fig. S3, and the possible deterioration of model performance. In this example, a strong constraint (5.13) is imposed on the test functions and this is considered to have resulted in the less expressive model whereas the model training becomes robust while keeping satisfactory model performance for other controller design tasks.

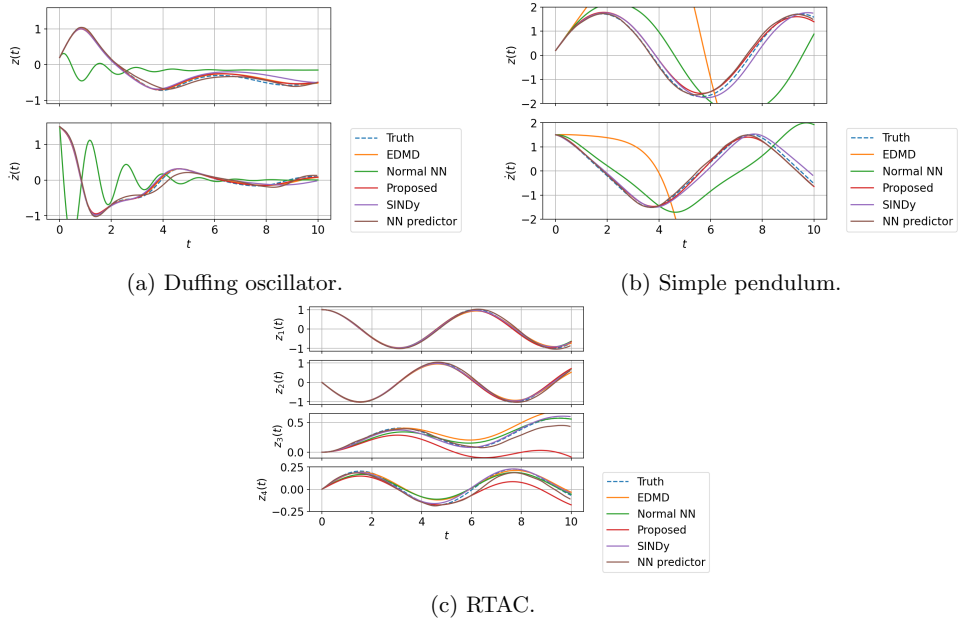


Fig. S5: Comparison of state predictive accuracy.

References

- [1] S. L. BRUNTON, J. L. PROCTOR, AND J. N. KUTZ, *Discovering governing equations from data by sparse identification of nonlinear dynamical systems*, Proceedings of the National Academy of Sciences, 113 (2016), pp. 3932–3937.
- [2] S. L. BRUNTON, J. L. PROCTOR, AND J. N. KUTZ, *Sparse identification of nonlinear dynamics with control (SINDYc)*, IFAC-PapersOnLine, 49 (2016), pp. 710–715.